Lithospheric-scale extension during Grampian orogenesis in Scotland

DANIEL R. VIETE[1]*, SIMON W. RICHARDS[2], GORDON S. LISTER[1],
GRAHAME J. H. OLIVER[3] & GRAHAM J. BANKS[4]

[1]*Research School of Earth Sciences, Australian National University, Canberra
ACT 2601, Australia*

[2]*School of Earth and Environmental Sciences, James Cook University, Townsville,
QLD 4811, Australia*

[3]*School of Geography and Geosciences, University of St. Andrews, St. Andrews,
Fife KY16 9AL, UK*

[4]*School of Earth, Ocean and Planetary Sciences, Cardiff University, Cardiff CF10 3YE, UK*

*Corresponding author (e-mail: daniel.viete@anu.edu.au)

Abstract: This contribution presents a new model for the Grampian-age tectonothermal development of the Buchan Block and Barrovian-type regions to its west, in the Grampian Terrane, Scotland. The model has drawn on evidence gathered from field mapping, microstructural analysis, metamorphic petrology and mafic magma geochemistry to propose that emplacement of the Grampian gabbros and regional metamorphic heating associated with production of Barrovian- and Buchan-type units occurred during syn-orogenic (Grampian-age), lithospheric-scale extension. Extension followed lithospheric thickening associated with the initiation of Grampian orogenesis and was followed by renewed lithospheric thickening and termination of the extensional heating. Mantle melting to produce the Grampian gabbros of the Grampian Terrane was achieved by extensional thinning of the lithosphere and decompression melting of the asthenosphere at depths of less than 70 km. Advection of heat from the mantle with emplacement of the Grampian gabbros augmented elevated heat budgets associated with attenuation of isotherms during extension. Deposition of the uppermost Dalradian (the Whitehills and Boyndie Bay Groups and the Macduff Slates) occurred during Grampian-age lithospheric extension. A gently-dipping, mid-crustal detachment focused metamorphic heat sources and accommodated significant lithospheric-scale strain, allowing independent thermal evolution of units in its hanging wall (the Buchan Block) and footwall (Barrovian-type units).

Barrovian- and Buchan-type metamorphism represent two classic examples of metamorphism associated with certain mineral assemblages in pelites and corresponding trajectories in pressure–temperature ($P–T$) space (Fig. 1). The terms Barrovian metamorphism and Buchan metamorphism appeared in the geological literature following the work of Barrow (1893, 1912) and of Read (1923, 1952), respectively, in the Grampian Terrane, Scotland. Barrow and Read each observed systematic changes in the mineral assemblage preserved in pelitic lithologies with space, which they interpreted to indicate changes in the metamorphic conditions to which the rocks were subjected. Barrovian- and Buchan-type metamorphic sequences are commonly found at convergent plate boundaries and conditions responsible for production of these metamorphic assemblages emerge from thermotectonic processes that operate in these settings.

The classical Barrovian metamorphic sequence described by Barrow (1893, 1912) crops out in the SE of the Grampian Terrane, Scotland, immediately NW of the terrane-bounding Highland Boundary Fault (HBF) (Fig. 2a). The sequence is typified by the successive appearance of chlorite, biotite, garnet, staurolite, kyanite and sillimanite with increasing metamorphic grade, from SE to NW (Fig. 2a). Metamorphic units of the Grampian Terrane that occur west of the classical sequence of Barrow (1893, 1912) and west of the Portsoy-Duchray Hill Lineament (PDHL) of Fettes *et al.* (1986) also experienced metamorphism along Barrovian-type $P–T$ trajectories during Grampian orogenesis.

The type locality for the Buchan metamorphism described by Read (1923, 1952) occurs within the Ythan Valley, SE of the Kirktown of Auchterless in Aberdeenshire (Fig. 3). The sequence preserves
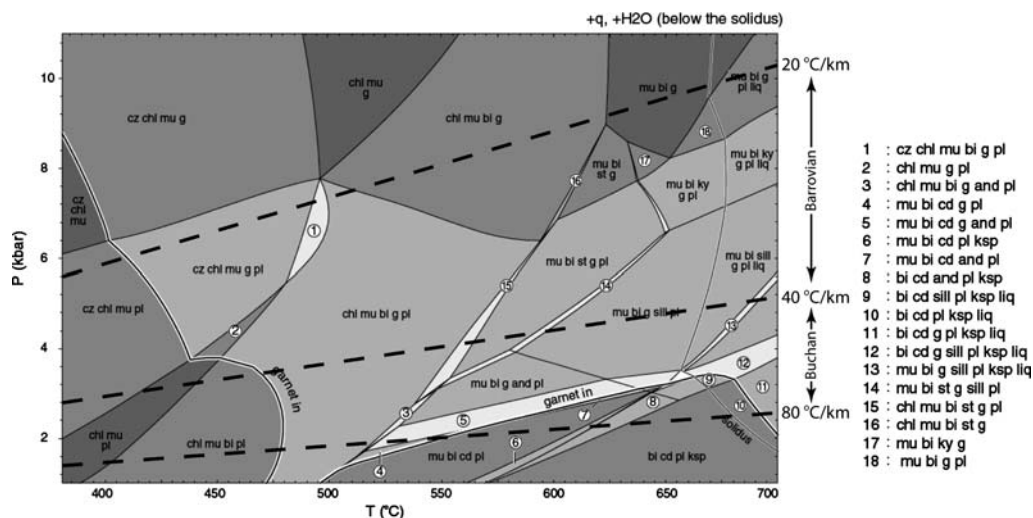
Fig. 1. Typical-pelite MnNCKFMASH pseudosection from Boger & Hansen (2004, p. 520, fig. 5a) with fields for Barrovian- and Buchan-type metamorphism in *P–T* space, as defined from estimates made for the *P* and *T* of metamorphism in the east of the Grampian Terrane (Harte & Hudson 1979; Hudson 1985; Baker 1985; Beddoe-Stephens 1990; Zenk & Schulz 2004). Abbreviations include: and, andalusite; cd, cordierite; chl, chlorite; cz, clinozoisite; g, garnet; H2O, water; ksp, K-feldspar; ky, kyanite; liq, liquid; mu, muscovite; pl, plagioclase; q, quartz; sill, sillimanite; st, staurolite.

biotite, cordierite, andalusite and sillimanite with increasing metamorphic grade (Fig. 2a). Staurolite also appears in andalusite- and sillimanite-grade rocks of Buchan-type metamorphic sequences west of the classical example (Fig. 2a). Units that preserve Buchan-type metamorphic assemblages within the Grampian Terrane are restricted to regions east of the PDHL (Fig. 2a) and north of the sillimanite isograd that demarcates the northern extent of the classical Barrovian series in the SE (Fig. 2a). The Buchan-type metamorphic units of the Grampian Terrane define a discrete lithostratigraphic 'block' in the NE of the Grampian Terrane, referred to as the Buchan Block (Fig. 2a). Evidence for Grampian-age (*c*. 470 Ma) magmatism within the Grampian Terrane is restricted to the Buchan Block (Fig. 3). Voluminous granite and gabbro plutons occur in association with large-scale shear zones (Ashcroft *et al.* 1984), the most prominent of which, the PDHL, forms the western boundary to the Buchan Block.

A study of the transition between Barrovian- and Buchan-type metamorphic units of the Grampian Terrane was initiated to explore their relative timing of development and the tectonic setting within which they were produced. The study has focused on the structural and metamorphic history of the units that crop out between kyanite-zone units at Logie Head and biotite-zone units of the Buchan-type units at Macduff (Fig. 2b). The

transect (Portsoy transect) incorporates the PDHL, which marks the transition between Barrovian- and Buchan-type units on the coast at Portsoy (Fig. 2a). Whole-rock geochemistry of the igneous units at Portsoy has provided additional information to constrain the tectonic setting of their emplacement. A model that places development of the Barrovian- and Buchan-type metamorphic units of the Grampian Terrane within a tectonic and magmatic framework is proposed based on the structural, metamorphic and igneous evidence that is presented.

Geological background

Structure

Similar to other parts of the Grampian Terrane, the structure of the Buchan Block has been interpreted as having a nappe style of architecture. Read (1955) proposed that, on the basis of lithological and structural relationships exposed on the east–west trending Aberdeenshire coast around Banff, the Buchan Block was dominated by a large-scale, ESE-facing recumbent fold structure he termed the Banff Nappe. The nappe model of Read (1955) suggested that the upper limb of the Banff Nappe was removed along a tectonic dislocation known as the Boyne Line. The Boyne Limestone, Whitehills and Boyndie Bay Groups and the Macduff
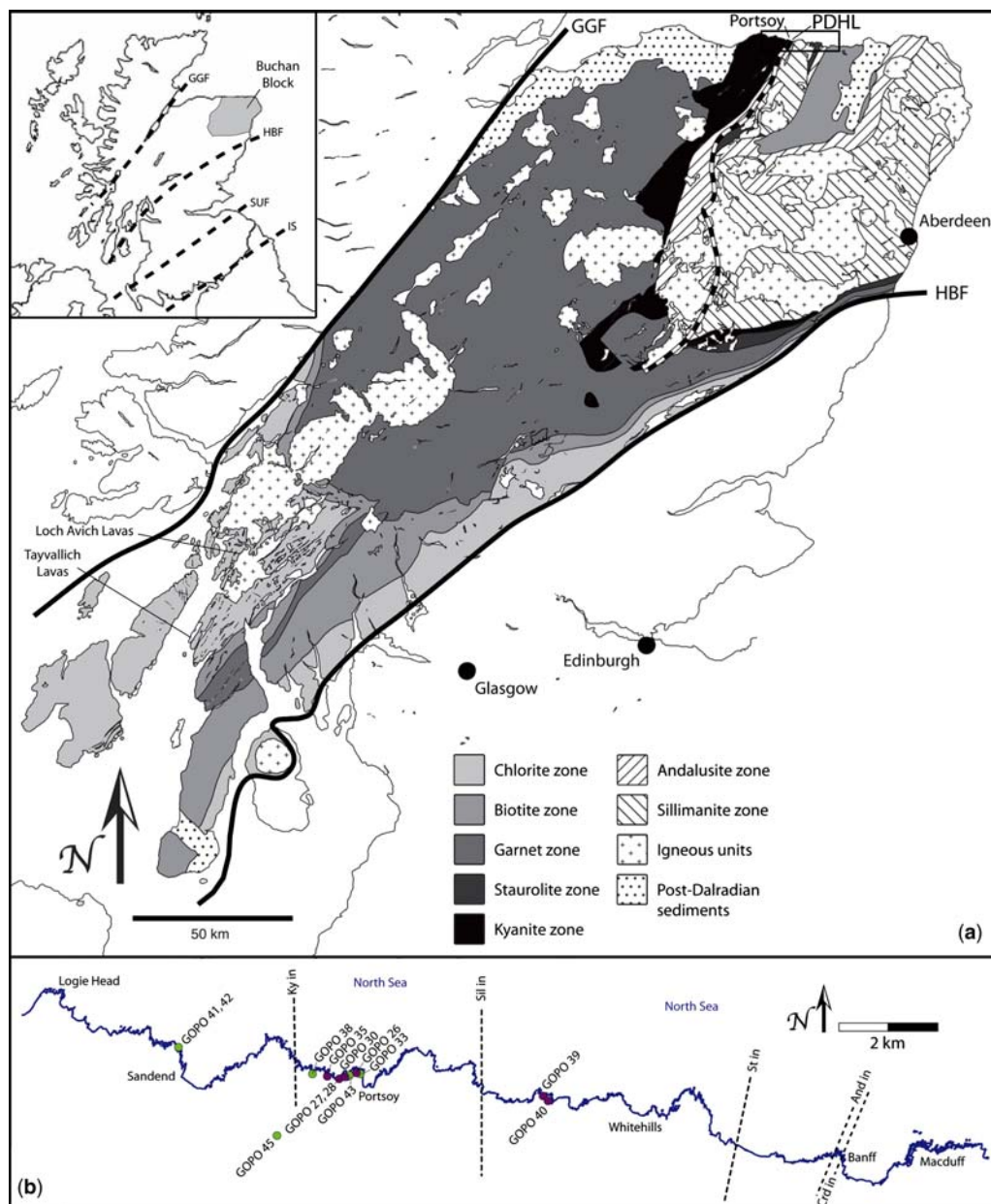
Fig. 2. Map of the Grampian Terrane, Scotland, showing (**a**) the distribution of metamorphic mineral isograds, magmatic bodies and post-Grampian sediments, and (**b**) localities for whole-rock samples from the Portsoy transect (enlargement of rectangle indicated on Fig. 2a. Inset at top left of Fig. 2a provides a broader location map and shows the Buchan Block within the Grampian Terrane). GGF, Great Glen Fault; HBF, Highland Boundary Fault; IS, Iapetus Suture; PDHL, Portsoy-Duchray Hill Lineament; SUF, Southern Uplands Fault. Compiled after Barrow (1912), Elles & Tilley (1930), Hudson (1980) and Fettes *et al.* (1986). Mineral abbreviations follow the recommendations of Kretz (1983).
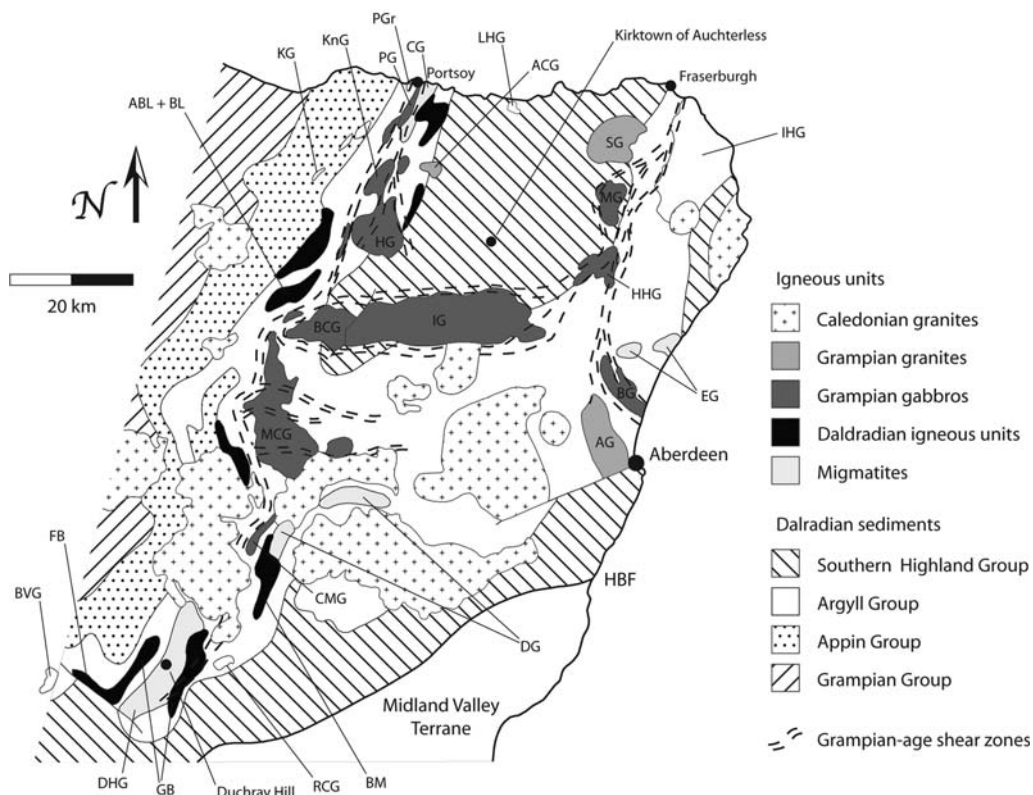
Fig. 3. Map of the Buchan Block displaying major magmatic bodies and Dalradian stratigraphic units after Ashcroft *et al.* (1984) and Goodman (1994). ABL + BL, Ardwell Bridge Lavas and Blackwater Lavas; AG, Aberdeen Granite; ACG, Aberchirder Granite; BCG, Boganclogh Gabbro; BG, Belhelvie Gabbro; BM, Balnacraig Metabasite; BVG, Ben Vuirich Granite; CG, Cowhythe Gneiss; CMG, Coyles of Muick Gabbro; DG, Donside Gneiss; DHG, Duchray Hill Gneiss; EG, Ellon Gneiss; FB, Farragon Beds; GB, Green Beds; HG, Huntly Gabbro; HHG, Haddo House Gabbro; IG, Insch Gabbro; IHG, Inzie Head Gneiss; KG, Keith Granite; KnG, Knock Gabbro; LHG, Longmanhill Granite; MCG, Morven-Cabrach Gabbro; MG, Maud Gabbro; PG, Portsoy Gabbro; PGr, Portsoy Granite; RCG, Rough Craig Granite; SG, Strichen Granite.

Slates were brought into contact with the gneissic core of the underlying nappe (the Cowhythe, Donside, Ellon and Inzie Head Gneisses) by movements along the Boyne Line. In Read's model, high-grade units exposed in association with high-strain zones in the regions of Portsoy and Fraserburgh on the Aberdeenshire coast represent surface breaching of the nappe core from beneath the right-way-up Dalradian metasediments that crop out in the intervening region. Isotopic (Rb–Sr) work carried out on the Ellon and Inzie Head Gneisses indicates that their metamorphism pre-dates Dalradian sedimentation (Sturt *et al.* 1977), and Ramsay & Sturt (1979) used this as evidence to propose an allochthonous origin for units of the Buchan Block, involving a basement-cover relationship between the Proterozoic gneisses and Ordovician metasediments brought into contact by movement

along the Boyne Line. G. J. H. Oliver (unpublished data) holds U–Pb zircon evidence to support the pre-Dalradian origin for the Cowhythe Gneiss proposed by Sturt *et al.* (1977) and Ramsay & Sturt (1979). Ashcroft *et al.* (1984) interpreted high-strain regions of the Buchan Block as representing long-lived shear zones responsible for the lithostratigraphic juxtapositions that Read (1955) observed, thereby refuting the nappe model. The Ashcroft *et al.* (1984) model interprets the Buchan Block as autochthonous to the surrounding Dalradian, its unique character within the Grampian Terrane related to the proposed vertical transposition of the block, relative to neighbouring regions, along the major shear zones that surround it.

The importance of shear zones in the tectonic development of the Grampian Terrane, and in particular in the Buchan Block, is well documented

(e.g. Ashcroft *et al.* 1984; Fettes *et al.* 1986, 1991; Baker 1987; Goodman 1994). Ashcroft *et al.* (1984) first described an extensive network of shear zones within the Buchan Block that host large, syn-deformational igneous intrusive bodies (Fig. 3). These thin zones of intense strain are coincident with changes in lithostratigraphy, and divide regions with different structural histories. The most significant shear zone in the NE of the Grampian Terrane defines the western boundary of the Buchan Block (Fig. 2a), and is referred to in the literature as the Portsoy–Duchray Hill Lineament (PDHL). The PDHL has been mapped as a feature that is variable in thickness along its length, but continuous for over 100 km.

Fettes *et al.* (1986) revealed the true significance of the PDHL. They demonstrated a spatial relationship between a number of sudden changes in the geology, geochemistry and geophysics of the Grampian Terrane with a zone of intense shear deformation that winds from Portsoy, approximately SSW, to Duchray Hill (Fig. 3). The shear zone incorporates a number of variably dismembered gneissic and igneous bodies, some of which predate Grampian tectonism, and others that intruded into, or developed within, the zone of active shearing during Grampian orogenesis. Igneous units are so abundant within the PDHL that the shear zone can be traced, in regions of poor outcrop, using magnetics alone (Fettes *et al.* 1991). Regional surveys carried out by the British Geological Survey have demonstrated discrete differences in the geochemistry and gravity response of units either side of the PDHL (Fettes *et al.* 1986). The gravity map of Figure 4 demonstrates clearly the distinct nature of the Buchan Block with respect to neighbouring Grampian regions in the anomalously high gravity response of the Buchan Block. Stratigraphic units are disrupted by the presence of the PDHL, and interpreted excision of stratigraphy has been proposed as further evidence for a significant movement history associated with the shear zone (Fettes *et al.* 1991). Evidence for antiquity of the feature may lie in the rapid lateral facies variations that occur within the region of the PDHL, consistent with activity of the feature during Late Proterozoic deposition of Dalradian sediments (Fettes *et al.* 1986, 1991). Most importantly for this work, the PDHL marks the transition between the Barrovian- and Buchan-type metamorphic units at the western boundary of the Buchan Block (Fig. 2a). In addition to defining a break in the metamorphic pattern, the PDHL has influenced the location of sillimanite- and migmatite-grade units (Kneller & Leslie 1984).

A broad zone of partitioned shear defines the PDHL, within which units vary in strain intensity, from relatively undeformed to ultra-mylonitic. A number of discrete, sub-vertical shear zones have been recognized, the most well known of which are the Portsoy Thrust of Elles (1931) and the Boyne Line of Read (1955). These shear zones are visible in coastal exposures of the PDHL near Portsoy, and define distinct Grampian-age shear planes. The structure of the PDHL records an extensive movement history with a dominantly top-to-the-east normal-sense (Ashcroft *et al.* 1984) or top-to-the-west thrust-sense movement (Baker 1987; Beddoe-Stephens 1990; Dempster *et al.* 1995). Careful structural mapping carried out by Carty (2001) revealed that kinematic indicators with both top-to-the-east and top-to-the-west movement sense occur within the PDHL at Portsoy. Movement along the Portsoy Thrust and Boyne Line appears to have resulted in significant excision of stratigraphy west of Portsoy, evidenced by the fact that these features bound the potentially basement-derived Cowhythe Gneiss unit (Ramsay & Sturt 1979; G. J. H. Oliver unpublished data).

Late, open folding of Buchan Block lithologies formed a NNE-trending, synclinal/anticlinal fold pair known as the Turriff Syncline and Buchan Anticline (Read & Farquhar 1956). Axial traces of the late folds are defined in the isobaric pattern preserved by the regional metamorphism (Chinner 1966; Harte & Hudson 1979; Baker 1987; Fig. 5). Metamorphic isograds of the Buchan Block appear to cut the late folds, suggesting that thermal relaxation followed the fold movements and thus that late folding commenced prior to cooling of the country rocks (cf. Read & Farquhar 1956). The relationship between pressure and temperature distribution in the NE of the Grampian Terrane is illustrated by the isobar/isotherm maps of Chinner (1966) and suggests that the inferences of Read & Farquhar (1956) concerning the timing of metamorphism with respect to late folding were correct. Conversely, the isobars and isotherms of Harte & Hudson (1979) and Baker (1987) for the NE of the Grampian Terrane display a congruence that suggests post-metamorphic formation of the Turriff Syncline and Buchan Anticline. Observations, in the field, of lithologies that have been cross-cut by isograd boundaries have been made for folds related to the Boyndie Syncline in units of the Banff division (Sutton & Watson 1956).

The Boyndie Syncline is a large scale, monoformal fold whose hinge zone lies immediately west of Banff. Early workers assigned the Boyndie Syncline an early Grampian structural timing (Sutton & Watson 1956), on the basis of structural changes observed between its steeply-dipping western and gently-dipping eastern limbs. In a later revision, the timing of the folding that formed the Boyndie Syncline was deemed equivalent to that for the development of the Turriff Syncline and Buchan Anticline (Johnson & Stewart 1960; Johnson
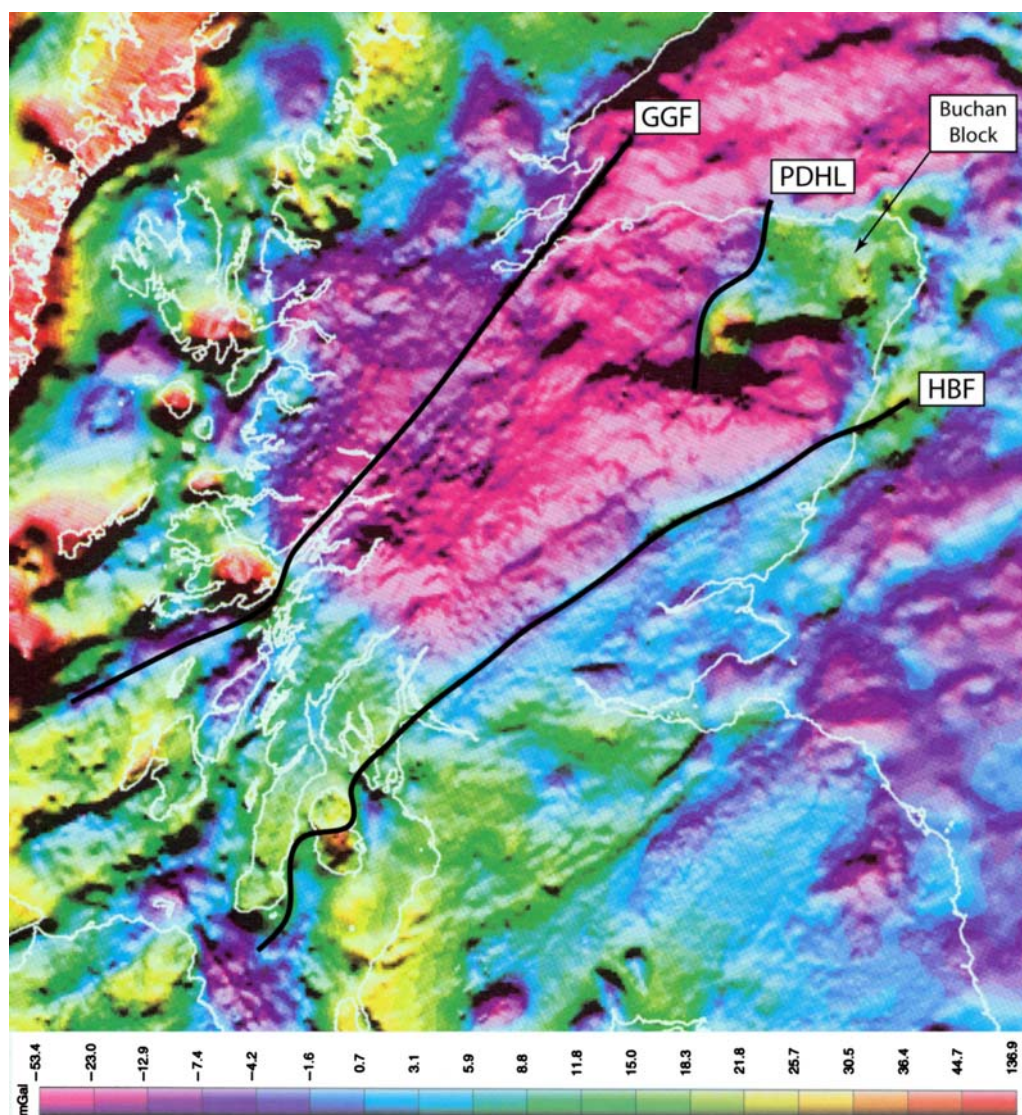
Fig. 4. Annotated shaded relief image of the gravity anomaly map of the Grampian Terrane, Scotland, (after Trewin & Rollins 2002, p. 17, fig. 1.7). Bouguer gravity anomaly onshore, and free-air anomaly offshore is illuminated by a sun angle of 45° from the north. Colour scheme relates to gravitational acceleration (in mgal) measured from gravitational surveys (calibration bar located beneath the map). GGF, Great Glen Fault; HBF, Highland Boundary Fault; PDHL, Portsoy-Duchray Hill Lineament.

1962; Fettes 1970). Later, Treagus & Roberts (1981) concluded that the fold set is an early, rather than a late feature. Stephenson & Gould (1995) have also questioned the age of the Turriff Syncline and Buchan Anticline, contending that one, or both, may have developed later than suggested by calculations based on conventional models for structural development of the Buchan Block. Much confusion still surrounds the structural

timing of large folds of the Buchan Block, in particular the Boyndie Syncline.

Magmatism

Read (1919) divided the mafic igneous units of Aberdeenshire into an 'older' series and a 'younger' series on the basis of differing strain intensity. More recent mapping has shown that
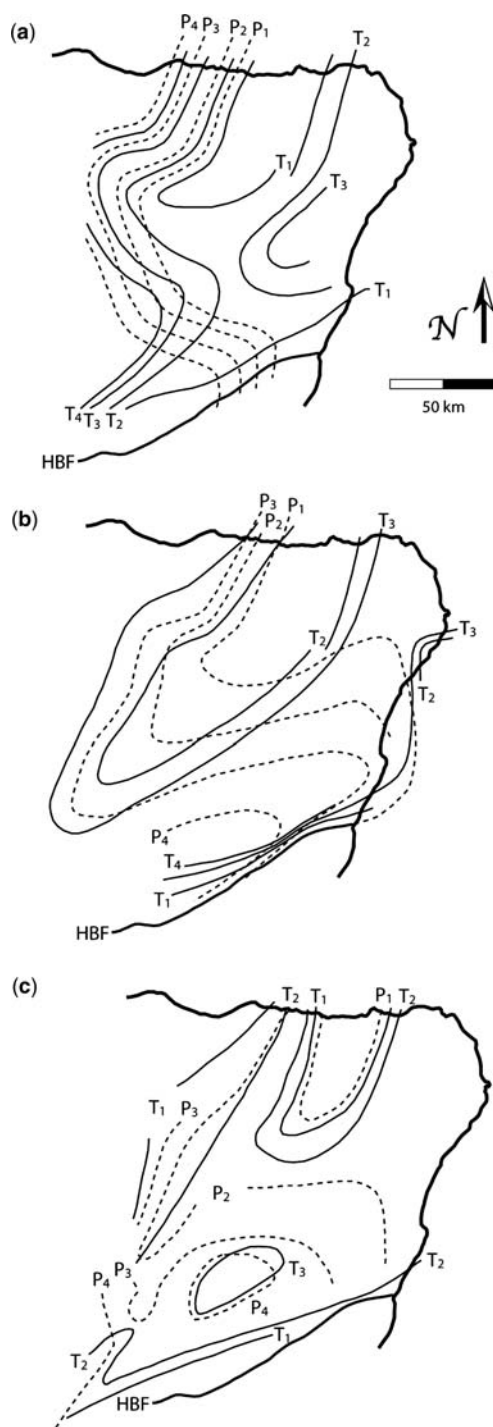
Fig. 5. Pressure–Temperature distribution maps produced by (**a**) Chinner (1966), (**b**) Harte & Hudson (1979) and (**c**) Baker (1987) for the NE of the Grampian Terrane.

some mafic igneous units assigned an 'older' age by Read (1919) are in fact deformed members of the 'younger' series (Leslie 1984; Munro & Gallagher 1984). Lithostratigraphical and geochronological studies support the early interpretation of Read (1919), which holds that two episodes of mafic magmatism occurred. For the purpose of this study, igneous units belonging to Read's (1919) 'older' series are prefixed with 'Dalradian' whereas units of his 'younger' series are prefixed with 'Grampian'. Post-Grampian felsic magmatic units that are abundant within the Grampian Terrane are referred to in the following sections as 'Late-Caledonian' units. All igneous bodies mentioned in the following sections can be located on Figure 3.

Dalradian magmatism. The Dalradian magmatic units of the Grampian Terrane include all igneous units that crystallized prior to the first phase of the deformation associated with the Grampian Orogeny (*sensu* Lambert & McKerrow 1976). They comprise a series of Precambrian, syndepositional (Dalradian-age) mafic- and ultramafic-volcanic and sub-volcanic units and a series of felsic intrusive bodies, referred to here as the Dalradian metabasites and Dalradian granites, respectively.

Volcanic and sub-volcanic mafic and ultramafic units of Dalradian age are recognized across the Grampian Terrane, for example, the Tayvallich and Loch Avich Volcanics of Argyllshire (Wilson & Leake 1962; Graham 1976); the Portsoy Metabasites (this study), Ardwell Bridge Lavas (MacGregor & Roberts 1963) and Blackwater Lavas (Fettes & Munro 1989; Fettes *et al.* 1991) of Aberdeenshire; the Farragon Beds and Balnacraig Metabasites (Goodman & Winchester 1993) of Perthshire, and the Green Beds (van de Kamp 1970) of Perthshire and Argyllshire. At all of these localities, the metavolcanic units are situated within the upper Argyll Group stratigraphy, or at the base of the Southern Highland Group (McDonald *et al.* 2005). In the NE of the Grampian Terrane, the lithostratigraphic transition between the Argyll Group and the Southern Highland Group lies within the high-strain zone that forms the Portsoy-Duchray Hill Lineament (PDHL) of Fettes *et al.* (1986). Consequently, units of the Dalradian metabasites are commonly dismembered and display complex lithostratigraphic relationships with surrounding units. U–Pb dating of zircons from the Tayvallich Volcanics has revealed an eruption age of 595 ± 4 Ma (Halliday *et al.* 1989). This age is within error of a sensitive high-resolution ion microprobe (SHRIMP) U–Pb zircon age of 601 ± 4 Ma obtained from the Tayvallich Volcanics by Dempster *et al.* (2002), and suggests that these mafic volcanic units from the Dalradian stratigraphy were deposited at *c.* 600 Ma.

A number of granite bodies (including the Ben Vuirich and Rough Craig Granites of Perthshire and the Portsoy and Keith Granites of Aberdeenshire) occur in association with the Dalradian metabasites. The Dalradian granites display geochemical and isotopic signatures consistent with their classification as A-type granites (Tanner *et al.* 2006). The emplacement of A-type felsic rocks into the Dalradian series pre-dates the earliest deformation associated with the Grampian orogenic episode (Tanner 1996; Tanner *et al.* 2006), and is thought to have occurred during rifting associated with the break-up of Rodinia (Tanner *et al.* 2006). Geochemical analysis of pseudomorphed cordierite and andalusite (chiastolite) porphyroblasts in the contact aureole of the Ben Vuirich Granite was linked to the results of two-dimensional (2D) heat flow modelling to estimate the pressures and temperatures of the contact metamorphism (Ahmed-Said & Tanner 2000). The Ben Vuirich Granite was emplaced under ambient pressures of ≤ 2 kbar, producing a thermal perturbation that allowed country rocks to achieve temperatures of about 600 °C (Ahmed-Said & Tanner 2000). U–Pb dating of zircons from Dalradian granites has yielded emplacement ages of 590 ± 2 Ma (Rogers *et al.* 1989) and 597 ± 11 Ma (Pidgeon & Compston 1992) for the Ben Vuirich Granite, 600 ± 3 Ma (Tanner *et al.* 2006) for the Portsoy Granite and 601 ± 4 Ma (Tanner *et al.* 2006) for the Keith Granite. These studies indicate that the Dalradian granites were intruded at shallow crustal levels at *c.* 600 Ma, synchronous with mafic volcanism and the late stages of deposition of the Argyll Group sediments.

Grampian magmatism. Grampian magmatic units are defined here as all igneous units that carry evidence of Grampian age deformation, and that also demonstrably post-date the onset of Grampian orogenesis (*sensu* Lambert & McKerrow 1976). The Grampian-age magmatic suite includes both mafic and felsic intrusive units, referred to as the Grampian gabbros and Grampian granites, respectively. All Grampian-age igneous bodies are restricted to the NE of the Grampian Terrane, and occur in association with high-temperature, low-pressure (Buchan-type) metamorphism.

Major shear zones transect and bound bodies of the Grampian gabbros (Ashcroft *et al.* 1984). Movement immediately following emplacement of the igneous bodies is recognized on the major shear zones that host them (Ashcroft *et al.* 1984; Kneller & Leslie 1984), although the shear zones preserve a pre-Grampian deformation history (Fettes *et al.* 1986, 1991). The Grampian gabbros were emplaced during the regional metamorphism in the NE of the Grampian Terrane (Fettes 1970; Pankhurst 1970; Ashworth 1975), and also produced localized thermal effects that were superimposed on the regional metamorphic pattern (Fettes 1970; Pankhurst 1970; Ashworth 1975).

Studies carried out in the metamorphic aureoles of the Grampian gabbros of the Grampian Terrane suggest that contact metamorphism of country rock occurred at pressures of 4–5 kbar (*c.* 15–18.5 km) and temperatures between 700 and 850 °C (Droop & Charnley 1985). Fettes (1970) showed that the Grampian gabbros of the Buchan Block, collectively, constitute a deformed and disrupted 'sheet'. Droop & Charnley (1985) obtained identical depth-of-emplacement estimates for several bodies of the Grampian gabbros, suggesting that the Grampian gabbro sheet originated as a planar and sub-horizontal feature. Large-scale folding that followed peak metamorphism of the Buchan Block is held responsible for the current outcrop pattern of the Grampian gabbros (Fettes 1970).

U–Pb dating of zircon has produced age estimates of 470 ± 9 Ma for the Insch Gabbro (Dempster *et al.* 2002) and 471 ± 1.7 Ma (Carty *et al.* 2002) and 471.9 ± 2.4 Ma (Oliver *et al.* 2002) for the Portsoy Gabbro. Geochronology of the Grampian gabbros suggests that mafic magmatism occurred at *c.* 471 Ma.

A sequence of Grampian-age gabbroic bodies also occurs in the Dalradian of western Ireland. U–Pb zircon work has demonstrated that the emplacement ages of these gabbros -470.1 ± 1.5 Ma and 474.5 ± 1.0 Ma for the Cashel-Lough Wheelaun and Currywongaun Gabbros, respectively (Friedrich *et al.* 1999) – are identical to those of the Grampian gabbros. Like the Grampian gabbros, the gabbros of Connemara have been mapped as a folded and disrupted sheet (Thompson *et al.* 1985). The Irish gabbros display an identical timing of emplacement to the Scottish Grampian gabbros with respect to the structural and metamorphic history (Wellings 1998).

A number of Grampian-age granites crop out in association with the Grampian gabbros in the NE of the Grampian Terrane. The granites crystallized during regional metamorphism (Ashcroft *et al.* 1984; Kneller & Leslie 1984; Kneller & Aftalion 1987), were emplaced into major shear zones of the Buchan Block and are of a similar age to the Grampian gabbros. The Grampian granites display S-type characteristics including initial $^{87}Sr/^{86}Sr$ values of 0.710–0.720, peraluminous chemistry and inherited zircon populations (Pidgeon & Aftalion 1978; Harmon 1983). Johnson *et al.* (2003) used geochemical evidence to suggest that the Grampian granites formed by partial melting of the middle crust within the major shear zones that enclose the Grampian gabbros. Kneller & Aftalion (1987) demonstrated an emplacement age of 470 ± 1 Ma for the Grampian-age Aberdeen

Granite using U–Pb techniques on monazite. Dating of the Strichen Granite carried out by Pidgeon & Aftalion (1978) and Oliver *et al.* (2000) gave ages of 475 ± 5 Ma (U–Pb monazite) and 467 ± 6 Ma (U–Pb zircon), respectively. These two ages for the Strichen Granite are within error of each other and of the 470 ± 1 Aberdeen Granite age, suggesting an emplacement age of *c.* 470 Ma for the Grampian granites.

Late-Caledonian magmatism. Following Grampian orogenesis, widespread magmatic activity in the Caledonides of Britain and Ireland persisted until *c.* 400 Ma. Granite bodies emplaced after *c.* 460 Ma display no evidence of deformation or association with mafic magmatism in the Grampian Terrane and are classified as members of the Late-Caledonian granites (Oliver 2001). On the basis of geochronology and $^{87}Sr/^{86}Sr$ initial ratios, post-Grampian Late-Caledonian granites can be divided into two distinct groups (Oliver 2001). Early (*c.* 460–435 Ma) granites display S-type affinities and $^{87}Sr/^{86}Sr$ initial ratios identical to those for Grampian-age granites, whereas later (*c.* 435–400 Ma) granites yield markedly lower $^{87}Sr/^{86}Sr$ initial ratios and have I-type affinities. An association between the distribution of post-tectonic granites and the presence of major lineaments in the Grampian Terrane suggests that magmatism was either coeval with movement on these major shear zones (Jacques & Reavy 1994) or that pre-existing structures were utilized as migration pathways for magmatism (Oliver 2001).

Methods

Mapping approach

In the light of confusion caused by the application of classical nomenclature (D_1, D_2, D_3 . . .) to structural studies carried out in the Grampian Terrane (cf. Stephenson & Gould 1995) we have sought an alternative approach to deformation sequencing. For the presentation of the results of the structural study we have utilized a descriptive approach to labelling deformation fabrics and episodes similar to that outlined by Forster & Lister (2008) and Beltrando *et al.* (2008). It is felt that this alternative approach provides a more flexible structural framework into which new tectonic information can more easily be inserted.

Whole-rock geochemistry

Fresh material was chipped then crushed to a fine powder using a tungsten carbide mill. Glass disks, made by dissolution of the powders in molten lithium borate, were analysed for major element

abundance using a Spectro X-LAB 2000 energy dispersive X-ray fluorescence spectrometer equipped with a 3.0 kW Rh anode X-ray tube, housed at the School of Geography and Geosciences, University of St. Andrews. The accuracy of the method was better than $\pm 5\%$ (2σ) for major element analyses of the granitic rock standards GA and AC-E.

Trace element abundances were determined using the Perkin Elmer ELAN 5000 inductively coupled plasma mass spectrometer housed at the School of Earth, Ocean and Planetary Sciences, Cardiff University. Prior to analysis, powders were dissolved under pressure using acid (HF-HNO_3) digestion techniques. External precision for the instrument is better than $\pm 5\%$ (2σ) and the overall accuracy is better than $\pm 6\%$ (2σ), as determined from analyses of well known, internationally certified reference materials.
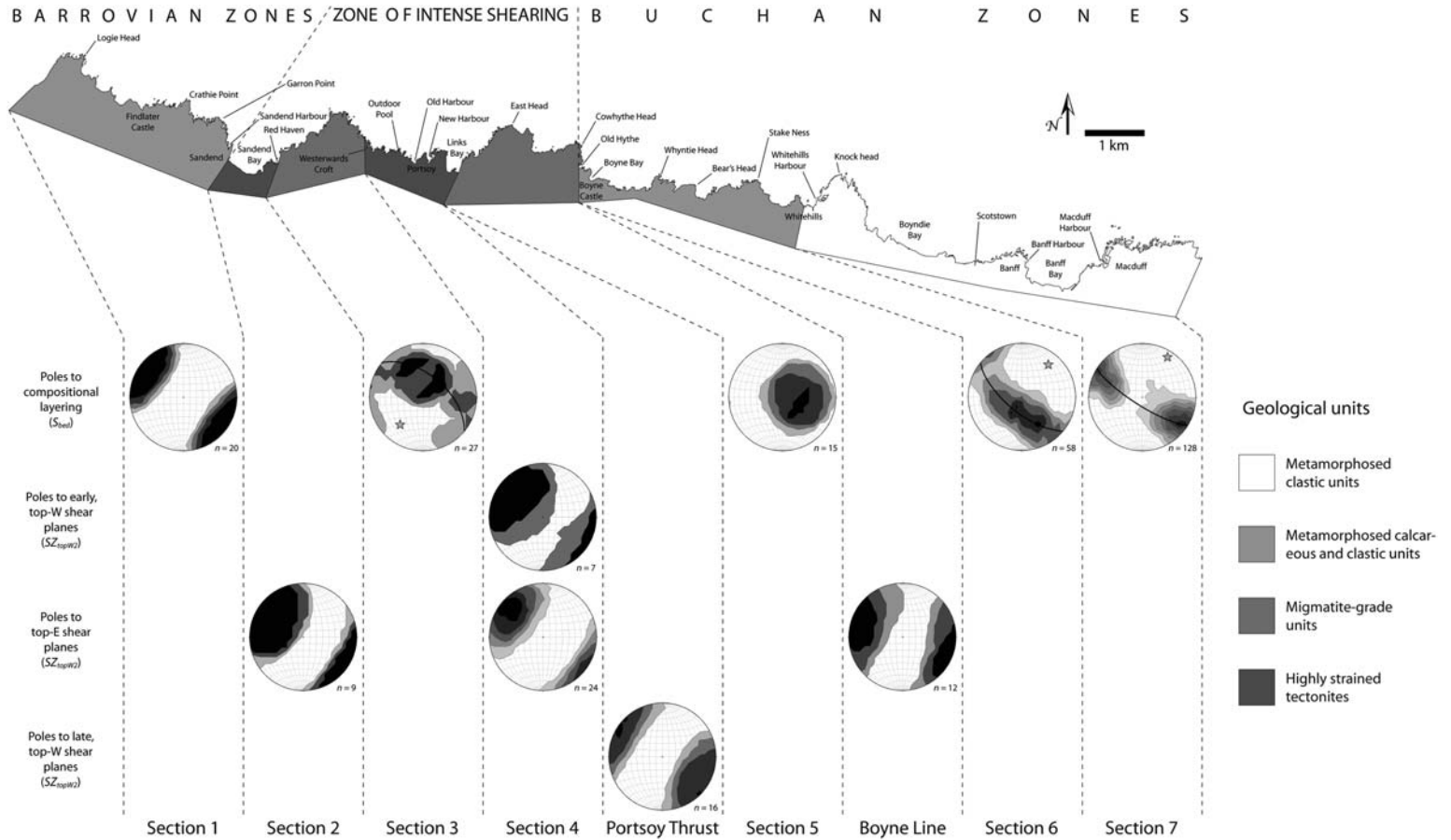
Structure of the Portsoy transect

To gain a better understanding of the chronology of sedimentation, metamorphism, magmatism and deformation that affected the NE of the Grampian Terrane, detailed mapping was carried out along a transect that stretches from Logie Head to Macduff (the Portsoy transect) on the Aberdeenshire coast (Fig. 2). Exposed in this transect are narrow (decametre wide) zones of intense shear that are coincident with broad changes in lithostratigraphy, deformation style and the structural history the rocks preserve (Fig. 6). Mapping identified seven discrete zones that preserve unique structural histories (Fig. 6). Correlation of structures across the seven sections are made in a summary of the regional structure of the Portsoy transect. Geographic locations referred to in the text are shown on Figure 6.

Results of mapping

Logie Head to Sandend – Section 1. The region between Logie Head and Sandend comprises a series of SW–NE trending units belonging to the Appin and Grampian Groups of the Dalradian Supergroup. Upsequence, toward the east from Logie Head, units become increasingly calcareous, passing from quartzites containing sporadic semi-pelitic and pelitic intercalations through flaggy psammites and pelites to the limestones that crop out in and around Sandend Harbour. At Garron Point, narrow actinolite schist units represent metabasic lithologies of volcanic or volcano-sedimentary origin (M_{act}).

Throughout Section 1, bedding maintains a steeply ($75–90°$) SE- or NW-dipping attitude. Early, bedding-parallel boudinage (D_{boudin}) is indicated by the presence of meta-limestone pods

Fig. 6. Map of the Portsoy transect displaying distinct structural domains identified from mapping, and stereographic projections of poles to fabrics mapped within them.

hosted in pelitic units of the Sandend Harbour region. Boudinaged beds are folded by a west-vergent, upright, close to open, subrounded fold generation (F_W) (Fig. 7a). Stereonet data in Figure 6 indicates that steep, long limbs dominate the fold structures, giving the fold envelope a steeply SE-dipping orientation. Two late fold generations defined as crenulations are observed in the section and are interpreted to represent a NE-trending, upright fold generation ($F_{upright}$) and a gently (25–35°) NW-dipping fold generation (F_{gentle}). Pelitic units from near to Logie Head carry both generations of crenulation, and cross-cutting relationships suggest that the upright generation post-dates the more gently-dipping generation. Garnetiferous semipelites from the Logie Head region display an additional fabric, which cross-cuts bedding and the layer-parallel fabric at a low angle, forming an intersection lineation that can be traced around hinges of folds of the upright, west-vergent fold generation. The fabric-forming event is labelled D_{la}. A structural sequence for the Logie Head to Sandend sequence can be written as follows:

$$B_{bed}M_{act}D_{boudin}D_{la}F_WF_{gentle}F_{upright} \qquad (1)$$

where B_{bed}, deposition event responsible for sedimentary layering; M_{act}, magmatism that formed protoliths to the actinolite schists; D_{boudin}, deformation responsible for layer-parallel boudinage; D_{la}, deformation represented by a foliation at a low angle to bedding; F_W, west-vergent folding; F_{gentle}, folding associated with a gently NW-dipping crenulations; and $F_{upright}$, folding associated with a late upright crenulation.

Sandend Bay – Section 2. According to Stephenson & Gould (1995), Sandend Bay represents the point where the Keith Shear Zone, which sits structurally below the Portsoy Shear Zone (PSZ), meets the coast. Outcrop is generally absent within the bay, although isolated occurrences of chiastolite schist show evidence of intense shear deformation. At the east side of Sandend Bay, outcrop commences with the appearance of semi-carbonitic psammites, which give way to a series of finely interbedded calc-silicates and psammites to the east that, despite the localized appearance of units of the post-Grampian Old Red Sandstone, persist to Red Haven.

Early layer-parallel boudinage (D_{boudin}) and rootless isoclinal folds (F_{iso}) occur parallel to bedding in the semi-carbonitic psammites and interbedded calc-silicates and psammites east of Sandend Bay. An intense, generally east- to SE-dipping (at 60–80°) layering exhibited within the section, post-dates layer parallel boudinage and appears to be associated with transposition of isoclinal folds. Strongly-aligned minerals along the shear plane are slightly oblique to the down-dip direction. Kinematic indicators (S-C fabrics, extensional shear bands and asymmetric clasts) in the plane normal to the shear plane and parallel to the mineral lineation indicate top-to-the-east shear movement. Top-to-the-east shearing within the Sandend Bay section is given the label SZ_{topE}. Locally, sheared units are folded by a tight, upright, west-vergent fold generation (F_W). An upright, NE-trending crenulation inferred to have formed during folding ($F_{upright}$) overprints the tight, west-vergent fold generation. The deformation sequence for the Sandend Bay section is as follows:

$$B_{bed}D_{boudin}F_{iso}SZ_{topE}F_WF_{upright} \qquad (2)$$

where B_{bed}, deposition event responsible for sedimentary layering; D_{boudin}, deformation responsible for layer-parallel boudinage; F_{iso}, isoclinal folding; SZ_{tope}, top-to-the-east shearing; F_W, west-vergent folding; and $F_{upright}$, folding associated with a late upright crenulation.

Red Haven to Westerwards Croft – Section 3. Rocks that crop out on the east side of Red Haven are distinct, lithologically, from those on the west side of the bay. They are of significantly higher metamorphic grade than those to the immediate west, and include quartzites, garnetiferous gneisses and migmatites. At the very east of Section 3, highly deformed, megacrystic granodiorites (members of the Portsoy Granite) crop out as narrow, bedding-parallel lenses of augen gneiss. The augen gneiss layers are rich in sedimentary xenoliths and, over short distances, exhibit varying degrees of influence of a mafic igneous component. The augen gneiss demarcates a transition between units of the PSZ to the east and higher-grade units (migmatites and gneisses) to the west. At GPS locality [NJ57896663], a break in the lithostratigraphy is apparent and a sudden change in lithology is observable across the augen gneiss, from migmatite in the west, to quartzite in the east. The contact is of probable tectonic origin. Events involving migmatization and gneissification of the metasedimentary units and intrusion of the granodiorite are assigned the labels D_{mig} and $M_{granite}$, respectively.

An early deformation parallel to, and observed to deform, (boudinage) migmatitic layering (D_{boudin}) defines tight to isoclinal, recumbent folds that, for the most part, are axial planar to compositional layering (F_{iso}) (Fig. 7b). West-vergent, open and subrounded folds with an axial plane that dips moderately (50–60°) ESE (F_W) post-date F_{iso} folds and are locally associated with west-directed, semi-brittle faults. Low-amplitude, north- to NE-trending, upright crenulations ($F_{upright}$) overprint all other structures. The augen gneiss that marks
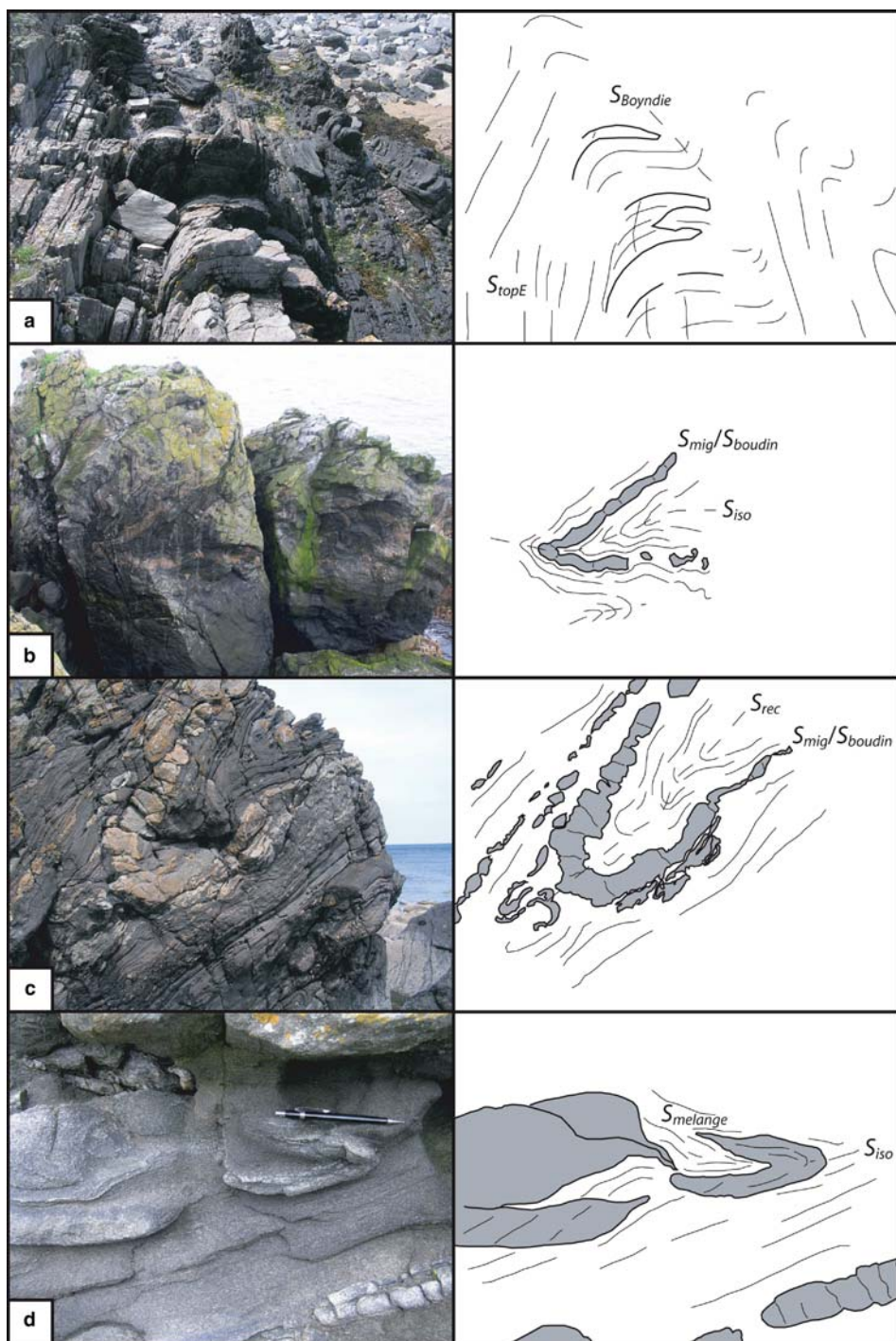
Fig. 7. Field photos from the Portsoy transect displaying (**a**) west-vergent $F_{Boyndie}$ folding of S_{topE} at Logie Head [GPS: NJ53176772, view to the SSW]; (**b**) a tight, recumbent F_{iso} fold of boudinaged migmatitic leucosome in the Durnhill Quartzite [GPS: NJ57256700, view to the WSW]; (**c**) a tight, recumbent F_{iso} fold of boudinaged migmatitic leucosome in the Cowhythe Gneiss [GPS: NJ60356688, view to the north]; and (**d**) an isoclinally-folded pod within the $S_{melange}$ fabric of the Cowhythe Gneiss [GPS: NJ61136652, view to the north].

the eastern edge of the section contains evidence of ductile shear along planes that dip at about $60°$ east and post-date F_{iso}, but pre-date semi-brittle deformation associated with F_W. The augen gneiss units preserve a down-dip lineation and S-C fabric relationships that suggest top-to-the-west movement. The shear deformation that affected the augen gneiss units is here labelled SZ_{topW}. Gneiss units at the western end of the section contain garnet porphyroblasts that have an included fabric defined by straight trails of quartz and mica. The orientation of the fabric is relatively uniform across grains and occurs at an angle to the main gneissic layering that wraps the garnets. The included fabric appears to pre-date all other fabrics on the section and is related to a deformation labelled D_{inc}. The following structural sequence is proposed for the section:

$$B_{bed}D_{inc}D_{mig}M_{granite}D_{boudin}F_{iso}SZ_{topW}F_WF_{upright} \quad (3)$$

where B_{bed}, deposition event responsible for sedimentary layering; D_{inc}, deformation represented by an included fabric in garnets; D_{mig}, deformation represented by migmatic layering and gneissosity; $M_{granite}$, magmatism associated with emplacement of the granite protolith to the augen gneiss; D_{boudin}, deformation responsible for layer-parallel boudinage; F_{iso}, isoclinal folding; SZ_{topW}, top-to-the-west shearing; F_W, west-vergent folding; and $F_{upright}$, folding associated with a late upright crenulation.

Westerwards Croft to Links Bay – Section 4. The region from the Portsoy Granite outcrop on the coast to the east side of Links Bay is characterized by thinned lithostratigraphy and the presence of variably deformed mafic and ultramafic units of the Grampian gabbros. The section as a whole is referred to as the PSZ. Within the PSZ, tectonic juxtaposition along a series of anastomosing shear zones has resulted in an interleaving of narrow units of varying character, including pelitic schists, highly-deformed quartzites, carbonitic metasediments, mafic metavolcanic rocks, serpentinites and variably-deformed gabbros (Fig. 8a). Strain partitioning is apparent and mylonites or mica-rich, high-strain units are commonly observed adjacent to, or wrapping, domains that have experienced less intense deformation. The eastern limit of the PSZ is defined by the most easterly occurrence of the highly deformed Grampian gabbros within Links Bay. The magmatic event related to emplacement of the gabbros is labelled M_{gabbro} and the event related to formation of the volcanic units is labelled M_{volc}.

Shear zones dominate the structure of the Portsoy section and exhibit conflicting shear sense indicators. Shear zone geometries are uniform and dip steeply $(75–85°)$ to the east to SE. Steep mineral and stretching lineations define an oblique movement direction and plunge $10–20°$ counterclockwise of the down-dip direction. Calcareous metasediments and quartzitic units preserve isoclinal folds (F_{iso}) of a bedding-parallel fabric that developed during an earlier deformation (D_{early}). Isoclinal fold hinges are variably reoriented by later shear and have hinge orientations that can range from horizontal to vertical at a single outcrop. Significant reorientation of early isoclinal fold hinges has resulted in the formation of spectacular mullion structures (Fig. 8a) that occur in the quartzite cliff faces immediately west of the Old Harbour. From Links Bay across the New Harbour to the east side of the Old Harbour, outcrop consists exclusively of variably deformed units of the Grampian gabbros. Mylonitic and ultramylonitic fabrics occur in the gabbros and are particularly well developed on the rock platforms to the north and east of the New Harbour and at the former dump site on the ridge that separates the New and Old Harbours. In less deformed regions, the gabbros take the form of relatively undeformed lenses wrapped by intensely deformed, hornblende schists (Fig. 9a). Both top-to-the-east (Fig. 9a) and top-to-the-west shear sense indicators, including S-C fabrics, extensional shear bands and asymmetric clasts or lenses (Fig. 9b), occur parallel to the stretching lineation, in rock faces perpendicular to the shear plane, in the gabbros. Top-to-the-west kinematic indicators in the gabbros post-date top-to-the-east kinematic indicators and are restricted in outcrop to regions to the west of the Old Harbour. Top-to-the-west kinematics in the gabbros, meta-carbonates and pelites that occur between the Old Harbour and the Outdoor Pool appear to post-date top-to-the-east observed in the same units. However, in the calc-silicate units that crop out on the west side of the Outdoor Pool, top-to-the-east kinematic indicators overprint top-to-the-west kinematic indicators. This suggests that top-to-the-west movement in the Portsoy section has both pre-dated and post-dated top-to-the-east movement and that the Portsoy section has accommodated multiple episodes of shear movement with opposing polarity. For the purpose of structural correlation, the early top-to-the-west, top-to-the-east and late top-to-the-west deformation events are labelled SZ_{topW1}, SZ_{topE} and SZ_{topW2}, respectively. Late folding of the S_{topE} shear fabric is preserved in pelites west of the outdoor pool. The folds (F_W) are moderately (about $40°$) SE-dipping and west-vergent and are associated with a dissolution cleavage and top-to-the-west thrusting (SZ_{topW2}). A NE-trending crenulation generation ($F_{upright}$) overprints the F_W folds. The
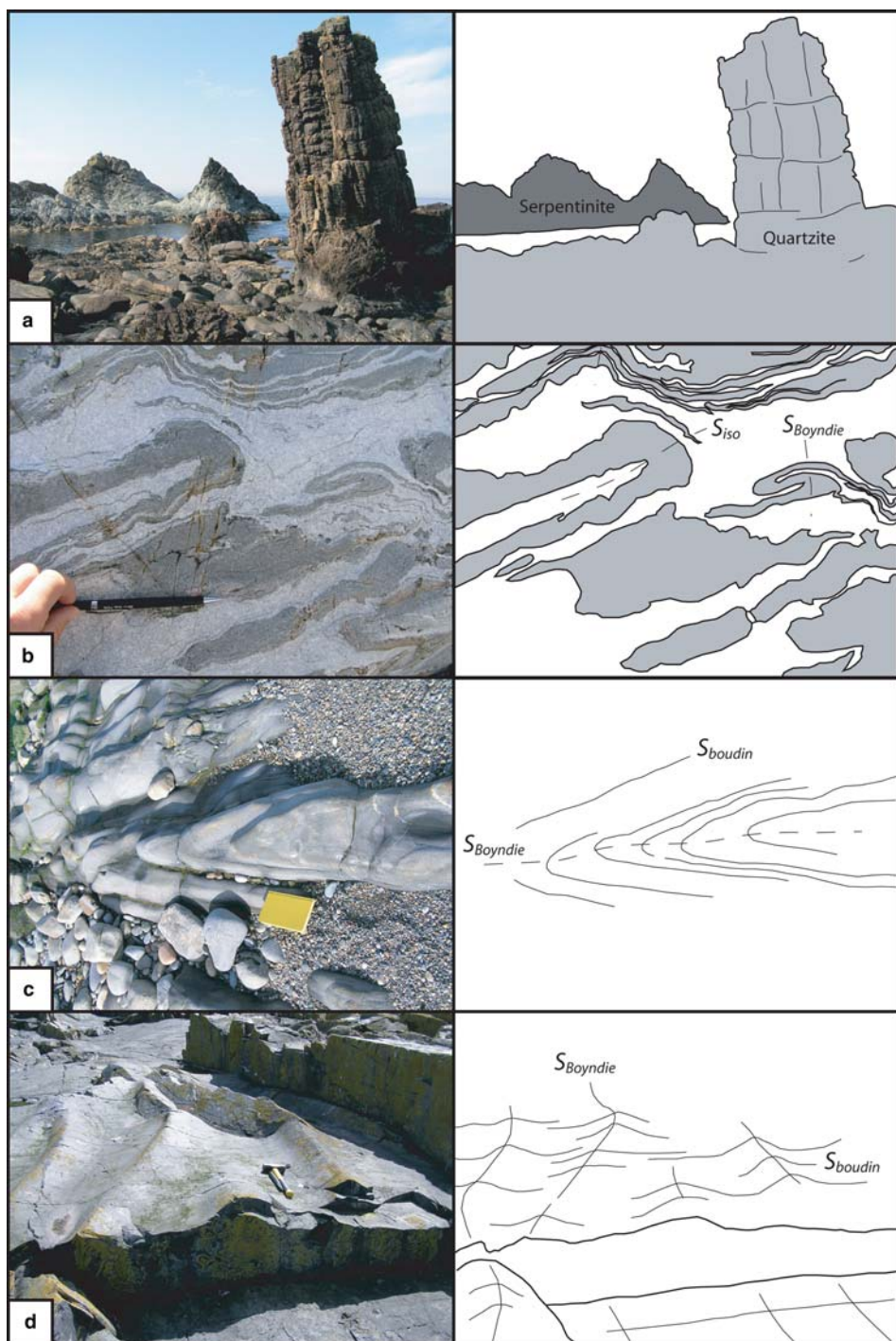
Fig. 8. Field photos from the Portsoy transect displaying (**a**) serpentinite and mullioned quartzite within the Portsoy Shear Zone [GPS: NJ58616632, view to the WNW]; (**b**) a refolded ($F_{Boyndie}$), boudinaged (D_{boudin}) and isoclinally folded (F_{iso}) marble layer in the Boyne Castle Limestone [GPS: NJ61556618, view to the SE]; (**c**) upright $F_{Boyndie}$ folds in andalusite-grade semi-pelites at Banff [GPS: NJ68316457, view down to the ESE]; and (**d**) upright $F_{Boyndie}$ folds in the biotite-grade slates at Macduff [GPS: NJ71386490, view to the SW].
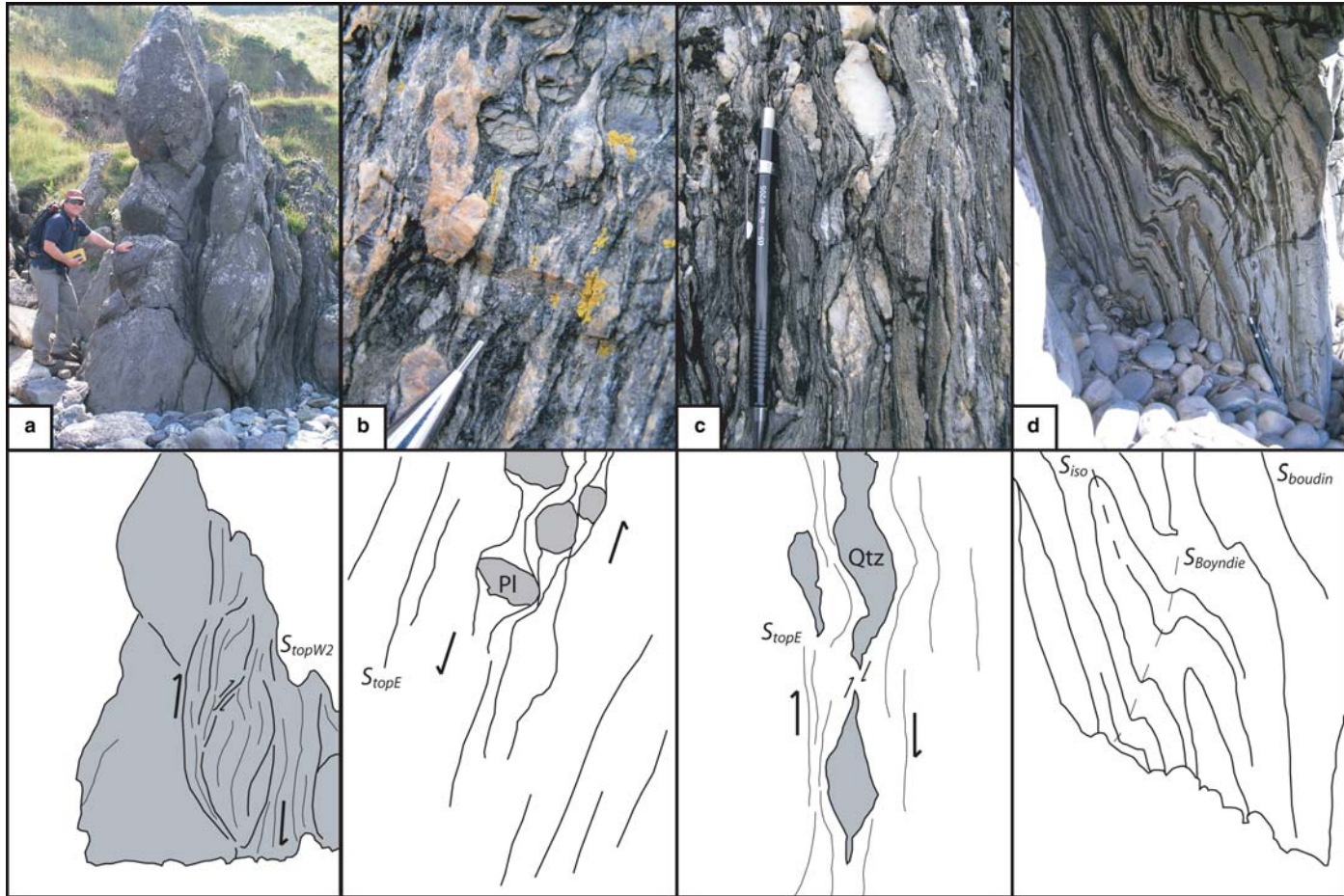
Fig. 9. Field photos from the Portsoy transect displaying (**a**) sheared mafic units of the Portsoy Gabbro body [GPS: NJ58526639, view to the WSW]; (**b**) a mylonitic amphibolite from the Portsoy Gabbro body [GPS: NJ58786637, view to the SSW]; (**c**) sheared asymmetric quartz lozenges from a highly-strained unit of the Boyne Line [GPS: NJ61556618, view NE]; and (**d**) isoclinally folded S_{boudin} refolded by $F_{Boyndie}$ [GPS: NJ61796598, view to the NE]. Mineral abbreviations follow the recommendations of Kretz (1983).

following deformation sequence describes the structural development of the Portsoy section:

$$B_{bed}M_{volc}D_{early}F_{iso}SZ_{topW1}M_{gabbro}SZ_{topE}F_WSZ_{topW2}F_{upright}$$
(4)

where B_{bed}, deposition event responsible for sedimentary layering; M_{volc}, volcanism that formed the protoliths to the metavolcanic units; D_{early}, deformation represented by the early layer-parallel fabric; F_{iso}, isoclinal folding; SZ_{topW1}, early top-to-the-west shearing; M_{gabbro}, magmatism related to emplacement of gabbros; SZ_{topE}, top-to-the-east shearing; F_W, west-vergent folding; SZ_{topW2}, late top-to-the-west shearing; and $F_{upright}$, folding associated with a late upright crenulation.

Links Bay to Old Hythe – Section 5. Sillimanite-grade, mylonitic semi-pelites and interbedded calc-silicate units crop out on the eastern shore of Links Bay. The highly deformed packages occur, locally, among high-grade, less-deformed migmatites and gneisses of the 'Cowhythe Gneiss'. Between Links Bay and Old Hythe, thin (*c.* 50 m thick) lenses of highly deformed calc-silicates and metabasic units disrupt the Cowhythe Gneiss. At Old Hythe, highly deformed migmatitic and sub-migmatitic gneisses give way, in an easterly direction, to lower-grade marbles and calc-silicates that record a less complicated deformation history. The transition occurs across a zone of mylonite, which appears to represent an important tectonic contact (the Boyne Line of Read 1955). Section 5 is characterized by the presence of high-grade (migmatitic) units and is bounded on both its western and eastern sides by thin zones that have experienced intense shear deformation. Development of migmatitic layering is assigned D_{mig} timing and the mafic magmatism that gave rise to the basic metavolcanic units is described as M_{volc}.

The Links Bay to Old Hythe section is dominated by pelites and semi-pelites, which at some stage achieved migmatitic grade. The migmatites of Cowhythe Head contain discrete leucosome and melanosome layers. The migmatitic units occur in association with an enigmatic, fine-grained rock type whose origins appear to lie in milling of the gneissic and migmatitic protoliths. The fine-grained rock type is formed of a biotite-rich matrix that hosts lenticular, relatively isotropic 'low strain' bodies (Fig. 7d) and is best described as a melange unit. A pre-Grampian shear deformation ($SZ_{melange}$) is held responsible for milling of the proto-gneissic and migmatitic units to produce the melange unit. Layer parallel boudinage (related to D_{boudin}) is observed in the relatively brittle leucosomes of the migmatitic units and, in places, defines tight to isoclinal recumbent folds (F_{rec}) whose axial planes are sub-parallel to the migmatitic layering (Fig. 7c).

Isoclines can also be observed in the melange units, and are defined by folding of elongate pods within the sheared matrix (Fig. 7d). On the east side of the section, mylonites in pelites and semi-pelites form the Boyne Line. The geometry of S-C fabrics and the asymmetry of quartz clasts (Fig. 9c) within units of the Boyne Line display an unequivocal top-to-the-east movement sense and the deformation is labelled (SZ_{topE}). Variably reorientated isoclinal fold hooks appear within the shear zone, suggesting that movement along the Boyne Line post-dates the early recumbent folding (F_{rec}). Across Section 5, early, gently-dipping fabrics are refolded by a west-vergent, upright, NNE-trending fold generation (F_W). On the west side of the section, the west-vergent, upright fold generation locally develops an axial planar dissolution cleavage in semi-pelites and is associated with intense, steeply-WNW-dipping (75–85°) shear zones and have a down-dip stretching lineation defined by the alignment of mica. Fabric and clast asymmetry in the plane perpendicular to the shear plane and parallel to the stretching lineation are consistent with top-to-the-west kinematics on late, F_W-related zones of movement (SZ_{topW}). Top-to-the-west shear is most intense at the western limit of the section, on the eastern edge of Links Bay (the location of the Portsay Thrust of Elles 1931). The shear fabrics of the Portsay Thrust are mylonitic in character and appear to have accommodated westward movement of the Cowhythe Gneiss relative to the units of the PSZ. An upright, NE-trending crenulation ($F_{upright}$) overprints all fabrics and represents the last deformation manifested in the structure of the units between Links Bay and Old Hythe. The deformation sequence for Section 5 can be written as follows:

$$B_{bed}D_{mig}SZ_{melange}M_{volc}D_{boudin}F_{rec}SZ_{topE}F_WSZ_{topW}F_{upright}$$
(5)

where B_{bed}, deposition event responsible for sedimentary layering; D_{mig}, deformation represented by migmatic layering; $SZ_{melange}$, shearing that formed the melange units; M_{volc}, volcanism that formed the protoliths to the metavolcanic units; D_{boudin}, deformation responsible for layer-parallel boudinage; F_{rec}, recumbent folding; SZ_{topE}, top-to-the-east shearing; F_W, west-vergent folding; SZ_{topW}, top-to-the-west shearing; and $F_{upright}$, folding associated with a late upright crenulation.

Old Hythe to Whitehills Harbour – Section 6. The Boyne Line at Old Hythe separates the migmatites and interleaved calc-silicates and limestones of the Cowhythe Gneiss from the Boyne Castle Limestone, which crops out in the bay area at Old Hythe. The Boyne Castle Limestone continues toward the east, despite breaks in its continuity

represented by thin, complexly deformed inter-bedded calc-silicate and semi-pelite units. East of Boyne Bay, the limestone increases in clastic material content and passes into a calc-silicate dominated sequence. An eastward transition from carbonate-dominated interbedded calc-silicates and semi-pelites to psammite-dominated lithologies corresponds with the appearance of gabbroic lenses (of M_{gabbro} age) and intense bleaching of country rock immediately east of Whyntie Head. Massive psammite with thin, interbedded and variously carbonitic semi-pelitic and pelitic layers continue to the east, toward the harbour region at Whitehills. Boudinaged, hornblende-rich metavolcanic units occur parallel to bedding in the region immediately east of Bear's Head and were emplaced during M_{volc}. With decreasing carbonate content in an easterly direction, andalusite becomes more prevalent. Units immediately west of Whitehills Harbour are dominated by highly-strained psammites that host gabbroic lenses of probable M_{gabbro} age, and contain abundant quartz veins interpreted to represented localized fluid fluxing during M_{gabbro}.

The deformation history of the Old Hythe to Whitehills Harbour section is appreciably simpler than that of Section 5 to the west. The outcrop pattern is controlled by tight to close, upright folding related to a fold generation that displays a consistent westerly vergence (F_W) (Fig. 9d). The fold generation can be traced eastward through the entire section from Old Hythe. In the ductile Boyne Castle Limestone Member (Fig. 8b) and transitional limestones to the east (Fig. 9d), layer-parallel boudinage (D_{boudin}), isoclinal folds (F_{iso}) and bedding define a west-vergent, open to close F_W fold generation. Eastward, the limestones increase in clastic material content and the sub-angular F_W folds of the limestone-rich units (Fig. 9d) become more sub-rounded. In the competent psammites of the region surrounding Bear's head, F_W folding forms broad, gentle closures. East of Stake Ness, the west-vergent folding is associated with a prominent dissolution cleavage in calcareous semi-pelites and commonly occurs in conjunction with small-scale, top-to-the-west thrusting (SZ_{topW}) along localized shear zones. Strong refraction of the cleavage occurs through the interbedded psammites and semi-pelites and the axial planar cleavage decreases in dip into semi-pelitic lithologies. In the Whitehills Harbour region, F_W occurs as sub-rounded, close to open closures in psammitic and semi-pelitic units.

At Stake Ness, bedding within a broad rock plat-form defines a large-scale, tight, antiformal closure whose axial plane dips at $30°$ to the west and is sub-parallel to compositional layering. The fold developed prior to the west-vergent folding (F_W), probably during the F_{iso} event.

The intertidal region immediately west of the harbour at Whitehills [GPS: NJ65376547] exposes gabbros of the M_{gabbro} event, quartz veins, small pockets of K-feldspar-bearing melts, an intense shear fabric with a white mica- and biotite-defined mineral lineation and top-to-the-east kinematic indi-cators. The fabric developed during top-to-the-east shear deformation (SZ_{topE}) prior to F_W. A late, upright NE-trending crenulation ($F_{upright}$) can be observed in pelitic units in the Whitehills region. The deformation sequence for the area can be written as follows:

$$B_{bed}M_{volc}D_{boudin}F_{iso}M_{gabbro}SZ_{topE}F_W SZ_{topW}F_{upright}$$

$$(6)$$

where B_{bed}, deposition event responsible for sedi-mentary layering; M_{volc}, volcanism that formed the protoliths to the metavolcanic units; D_{boudin}, defor-mation responsible for layer-parallel boudinage; F_{iso}, isoclinal folding; M_{gabbro}, magmatism related to emplacement of gabbros; SZ_{tope}, top-to-the-east shearing; F_W, west-vergent folding; SZ_{topW}, top-to-the-west shearing; and $F_{upright}$, folding associated with a late upright crenulation.

Whitehills Harbour to Banff and MacDuff – Section 7. Significant differences in character occur in the metasediments either side of Whitehills Harbour. East of the harbour, in the region of Knock Head, staurolite and andalusite-bearing metaturbidites occur in outcrop. Eastward, a grain size increase can be observed, with the turbidites becoming interbedded semi-pelitic and psammitic units. East of Boyndie Bay, psammites with interbedded, quartz-rich grit horizons give way to grey semi-pelites that are rich in cordierite. The units to the east of Boyndie Bay are of significantly lower meta-morphic grade than the staurolite-bearing units that occur in the Knock Head region. At Macduff to the east, units are again lower in metamorphic grade, cropping out as biotite-grade slates. Overall, a rapid decrease in metamorphic grade occurs east-wards from the west side of Boyndie Bay, with staurolite disappearing from the metamorphic assemblage over less than a kilometre. Less than another kilometre to the west, andalusite becomes absent and within another kilometre, across Banff Bay, cordierite disappears entirely.

The structure of the units to the west of Boyndie Bay is simple for the Portsoy transect. An early lithological layer-parallel deformation (D_{boudin}) has caused boudinage and disruption of bedding. The nature of D_{boudin} suggests that deformation occurred along the bedding plane of a partially con-solidated sedimentary sequence. In the upper parts of the Buchan Block stratigraphy, the initial defor-mation occurred soon after sediment deposition. Bedding and the layer-parallel fabric are folded

about close to open, sub-angular folds (Fig. 8c, d) with poles to bedding and S_{boudin} defining a great circle that denotes a regional upright fold generation whose hinges plunge at $12 \rightarrow 032$ (Fig. 6, Section 7). Vergence on the fold generation at Knock Head and to the west of Boyndie Bay is generally to the NW, in contrast to a SE vergence for the folds around Banff and Macduff. Vergence changes associated with the fold generation indicate the presence of a major synclinal closure in the proximity of Scotstown, near Banff [GPS: NJ67646489]. This structure represents the Boyndie Syncline of Sutton & Watson (1956), and the fold generation is accordingly labelled $F_{Boyndie}$. At Knock Head, west of Boyndie Bay and on the Banff foreshore, grading in turbidites and fold vergence on $F_{Boyndie}$ together indicate an upward facing on the $F_{Boyndie}$ axial plane. A late, upright NE-trending crenulation ($F_{upright}$) can be observed in pelitic units in the Whitehills region. The deformation sequence for the Banff and MacDuff section is:

$$B_{bed} D_{boudin} F_{Boyndie} F_{upright} \qquad (7)$$

where B_{bed}, deposition event responsible for sedimentary layering; D_{boudin}, deformation responsible for layer-parallel boudinage; $F_{Boyndie}$, upright folding and formation of the Boyndie Syncline; and $F_{upright}$, folding associated with a late upright crenulation.

Structural summary

Interpretation of the structure of the Aberdeenshire coast between Logie Head and Macduff requires correlation of structural episodes across the different structural domains. To begin with, a late upright crenulation is observed as the last deformation in all sections and is correlated with regional $F_{upright}$ folding. $F_{upright}$ was preceded by west-vergent, upright to slightly inclined folds (F_W of Sections 1–6), which are correlated with the $F_{Boyndie}$ fold generation of Section 7. This generation displays a broad vergence change across the Boyndie Syncline (from westerly on the west side to easterly on the east side). The regional folding is given the label $F_{Boyndie}$, after the large-scale syncline with which it is associated.

Gabbros in Sections 4 and 6 each display a similar timing during the Grampian orogenic episode and are correlated with the Grampian gabbros of the Grampian Terrane, labelled $M_{Grampian}$. Top-to-the-east shearing was observed in Sections 2, 4, 5 and 6, and in association with $M_{Grampian}$ on Sections 4 and 6. The structures associated with SZ_{topE} on each of these sections and D_{la} on Section 1 are correlated with a regional top-to-the-east shear episode (SZ_{topE}). Layer-parallel, soft-sediment deformation

in Section 7 is correlated with the layer-parallel, top-to-the-east shear deformation (SZ_{topE}) observed for Sections 2, 4, 5 and 6. The correlation between layer-parallel deformation (D_{boudin}) on Section 7 and SZ_{topE} elsewhere is made because there is no evidence to suggest that Section 7 escaped deformation associated with a number of deformation episodes that post-date SZ_{topE}.

Pre-SZ_{topE}, top-to-the-west shear manifested in the Portsoy Granite on Section 3 and in units of the Portsoy Shear Zone (Section 4) is assigned a regional SZ_{topW1} timing. Top-to-the-west shear that post-dates SZ_{topE} on Sections 4–6 is assigned a regional SZ_{topW2} timing. Early, lithological-layering parallel boudinage (D_{boudin}) is correlated across Sections 1–3, 5 and 6 and with the folded D_{early} of Section 4 to produce the regional D_{boudin} deformation. Tight to isoclinal folds (F_{iso} of Sections 2–4 and 6 and F_{rec} of Section 5) defined by lithological layering and the early S_{boudin} fabric are correlated with an early-Grampian regional folding event labelled F_{iso}. An F_{gentle} structural timing is assigned to the localized gently-dipping crenulation observed between F_W and $F_{upright}$ on Section 1.

Magmatism that pre-dates the regional D_{boudin} event, including M_{act} on Section 1, $M_{granite}$ on Section 3 and M_{volc} on Sections 4 to 6, is correlated with the Dalradian magmatism of the Grampian Terrane ($M_{Dalradian}$). Units formed during Dalradian magmatic activity at *c.* 600 Ma were emplaced (or deposited) prior to all activity associated with the Grampian orogenic episode and have proven useful time markers. Events that can be demonstrated to pre-date magmatism associated with $M_{Dalradian}$ can be reasonably classified as pre-Grampian. Sections 3 and 5 bear deformation that pre-dates $M_{Dalradian}$ and thus the Grampian orogenesis. Migmatitic layering and a gneissosity (D_{mig}) appear to have developed in these units prior to $M_{Dalradian}$ magmatism and are correlated with a regional migmatization event (D_{mig}). Pre-Grampian deformation that pre-dates (D_{inc}) and post-dates ($SZ_{melange}$) the D_{mig} deformation, can be observed for Sections 3 and 5, respectively.

Following structural correlation, it became apparent that B_{bed} for each of the mapped sections does not represent the same event. On Sections 3 and 5, B_{bed} pre-dates deformation events that themselves pre-date deposition of the metasediments of Sections 1, 2, 4 and 6 and associated volcanism of $M_{Dalradian}$ age (*c.* 600 Ma). According to the results of regional mapping, deposition of the metasediments of Section 7 occurred during the Grampian orogenic episode, while the effects of SZ_{topE} were being recorded in deeper parts of the Dalradian lithostratigraphy.

Overall, the Grampian orogenic episode, as it is documented in the rocks of the Portsoy transect,

involved eight regional deformations in addition to one episode of magmatism and one episode of sedimentation. Regions that were migmatized and made gneissose prior to the Grampian orogenesis have revealed at least three pre-Grampian deformation events. Deposition of the Argyll Group and the lower parts of the Southern Highland Group occurred between the pre-Grampian and Grampian age deformations, in association with emplacement of magmatic units of the Dalradian metabasites and granites ($M_{Dalradian}$). Table 1 summarizes the correlations in a regional deformation sequence diagram. The tectonic sequence proposed, including the timing of sediment deposition and magmatism in relation to deformation, holds a number of implications for the tectonic history of the region. The key points raised from mapping and production of the regional sequence diagram are:

(a) migmatite-grade units surrounding Portsoy preserve a structural history that appears to pre-date deposition of the Dalradian and all deformation events associated with the Grampian orogenic episode;

(b) structures that preserve evidence of shear deformation within the PSZ record changes in the polarity of shear movement – from top-to-the-west (SZ_{topW1}) to top-to-the-east (SZ_{topE}) to top-to-the-west (SZ_{topW2}) – during the Grampian orogenic episode;

(c) intrusion of the Grampian gabbros into shear zones of the Portsoy transect occurred during the top-to-the-east shearing (SZ_{topE});

(d) sediment deposition of the highest levels of the Dalradian stratigraphy (Whitehills and Boyndie Bay Groups and Macduff Slates) occurred during the SZ_{topE} deformation, during the Grampian orogenic episode, and

(e) the Boyndie Syncline and related folds preserve a similar late timing to that suggested by Johnson (1962) and Fettes (1970), rather than having formed as early structures (cf. Sutton & Watson 1956; Treagus & Roberts 1981).
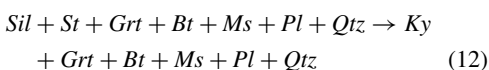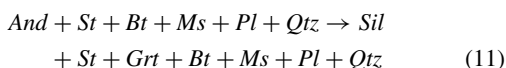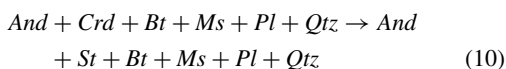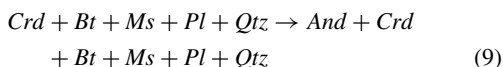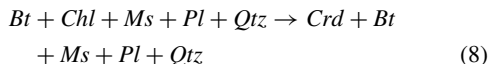
Metamorphism of the Portsoy transect

Across the Portsoy transect, changes in the metamorphic mineral assemblage preserved in pelitic units reflect changes in the temperature and pressure conditions that attended their metamorphism. Across-metamorphic-grade changes in the metamorphic assemblages and associated microstructures can provide information on the nature of the metamorphic heating that produced the Buchan-type units in relation to structural development and any evolution in metamorphic conditions during tectonic development.

Table 1. *Deformation correlation table and tectonic sequence diagram for the Portsoy transect, showing deformation sequences for each structural section and how they correlate*

Section	$B_{Grenville}$	D_{inc}	D_{mig}	$SZ_{melange}$	$B_{Dalradian}$	$M_{Dalradian}$	D_{boudin}	F_{iso}	SZ_{topW1}	$B_{Grampian}$	$M_{Grampian}$	SZ_{topE}	$F_{Boyndie}$	SZ_{topW2}	F_{gentle}	$F_{upright}$
1	$B_{Grenville}$	D_{inc}	D_{mig}	$SZ_{melange}$	B_{bed}	M_{ext}	D_{boudin}	F_{iso}				D_{lla}	$F_{Boyndie}$	SZ_{topW2}	F_{gentle}	$F_{upright}$
2					B_{bed}		D_{boudin}	F_{iso}	SZ_{topE}			SZ_{topE}	F_w		F_{gentle}	$F_{upright}$
3	B_{bed}	D_{inc}	D_{mig}			$M_{granite}$	D_{boudin}	F_{iso}	SZ_{topW1}				F_w			$F_{upright}$
4					B_{bed}	M_{volc}	D_{early}	F_{iso}			M_{gabbro}	SZ_{topE}	F_w	SZ_{topW}		$F_{upright}$
5	B_{bed}		D_{mig}	$SZ_{melange}$		M_{volc}	D_{boudin}	F_{rec}				SZ_{topE}	F_w	SZ_{topW}		$F_{upright}$
6					B_{bed}	M_{volc}	D_{boudin}	F_{iso}			M_{gabbro}	SZ_{topE}	F_w	SZ_{topW}		$F_{upright}$
7										B_{bed}		D_{boudin}	$F_{Boyndie}$			$F_{upright}$

Basement events — Dalradian events — Grampian events

Generalized mineral reactions 8–12 describe transitions in metamorphic mineral assemblage observed in the direction of increasing metamorphic pressure from the Buchan-type units through the PSZ and into the Barrovian-type units. Naturally, due to their dependence on bulk chemistry in addition to the conditions that prevailed during metamorphism, metamorphic assemblages that occur in the field do not always reflect the characteristic assemblages given below. Mineral abbreviations follow the recommendations of Kretz (1983).

$$Bt + Chl + Ms + Pl + Qtz \rightarrow Crd + Bt$$
$$+ Ms + Pl + Qtz \tag{8}$$

$$Crd + Bt + Ms + Pl + Qtz \rightarrow And + Crd$$
$$+ Bt + Ms + Pl + Qtz \tag{9}$$

$$And + Crd + Bt + Ms + Pl + Qtz \rightarrow And$$
$$+ St + Bt + Ms + Pl + Qtz \tag{10}$$

$$And + St + Bt + Ms + Pl + Qtz \rightarrow Sil$$
$$+ St + Grt + Bt + Ms + Pl + Qtz \tag{11}$$

$$Sil + St + Grt + Bt + Ms + Pl + Qtz \rightarrow Ky$$
$$+ Grt + Bt + Ms + Pl + Qtz \tag{12}$$

Results of the metamorphic study

Systematic changes in the timing of metamorphic mineral growth with varying metamorphic grade are recognized within the Buchan Block and across the PSZ. For this reason, the description of textures diagnostic of the structural timing of metamorphism is carried out separately for the different mineral zones. Figure 2a details the distribution of the different mineral zones.

Biotite zone. The biotite zone at Macduff has porphyroblasts that are partially aligned within the axial plane of $F_{Boyndie}$ folds and overgrow an earlier fabric (S_{topE}). Blastesis within the biotite zone of the Buchan Block appears to have occurred synchronous with development of upright folds belonging to the $F_{Boyndie}$ fold generation.

Cordierite zone. In thin section, cordierite porphyroblasts are inclusion rich and contain straight inclusion trails that define a weak fabric that postdates a layer-parallel fabric (Fig. 10a). The included fabric is continuous through the grain boundary into the matrix, appears most intense nearest to cordierite porphyroblasts and deflects slightly around cordierite grains (Fig. 10a). The early and late fabrics are both defined by white mica and biotite, suggesting that these minerals grew during these deformations. Correlation of fabrics in thin section with those observed in the field suggests that the early, layer-parallel fabric is the S_{topE} fabric and the later

fabric preserved within cordierite inclusion trails is the $S_{Boyndie}$ fabric. Biotite and white mica growth within the cordierite zone appears to have occurred syn-SZ_{topE} to syn-$F_{Boyndie}$, whereas cordierite growth timing within the cordierite zone can be restricted to syn-$F_{Boyndie}$.

Andalusite zone. Within the andalusite zone, white mica and biotite define a fabric that is sub-parallel to compositional layering and is axial planar to a later, upright crenulation. Correlation between fabrics observed in thin section and in the field suggests that the early layer-parallel fabric is S_{topE} whereas the later crenulation cleavage is related to $F_{Boyndie}$. Cordierite porphyroblasts have an included fabric that is defined by aligned white mica, biotite and quartz. This fabric displays a slight curvature in cordierite rims towards the external $S_{Boyndie}$ fabric.

Partial alignment of large andalusite porphyroblasts defines a down-dip mineral lineation on the S_{topE} plane. The andalusite mineral lineation can be traced around $F_{Boyndie}$ fold hinges, suggesting dominantly pre-$F_{Boyndie}$ growth timing. Inclusion trails within andalusite porphyroblasts occur in the orientation of the S_{topE} fabric, although, commonly, the internal fabric is deflected toward the external ($S_{Boyndie}$) fabric orientation at the outer edges of the crystal (Fig. 10b). Geometric relationships between fabrics included within porphyroblasts and external fabrics suggest the andalusite growth occurred during SZ_{topE} but overlapped with the initial stages of $F_{Boyndie}$. Andalusite porphyroblasts are strongly aligned within the axial plane of $F_{Boyndie}$ folds (Fig. 10d) but, in regions of lower $F_{Boyndie}$ strain, are less systematically aligned (Fig. 10e). Growth of white mica and biotite within the andalusite zone occurred during SZ_{topE} and into $F_{Boyndie}$ times. Andalusite and cordierite within the andalusite zone is assigned a late syn-SZ_{topE} to early syn-$F_{Boyndie}$ structural timing.

In terms of growth timing, andalusite within the andalusite zone of the Buchan Block is distinct from the andalusite that occurs in other areas of the Grampian Terrane, particularly in areas where kyanite has replaced earlier andalusite (Chinner & Heseltine 1979; Chinner 1980; Baker 1985; Beddoe-Stephens 1990).

Staurolite zone. Within the staurolite zone, staurolite and andalusite porphyroblasts have an included fabric, which is generally straight and at an angle to the external fabric, but displays slight curvature toward grain edges (Fig. 10c). Included fabrics in cordierite porphyroblasts are of the same generation and display similar geometric relationships to those included in staurolite and andalusite grains, suggesting a similar timing of growth for cordierite, andalusite and staurolite within the staurolite zone.
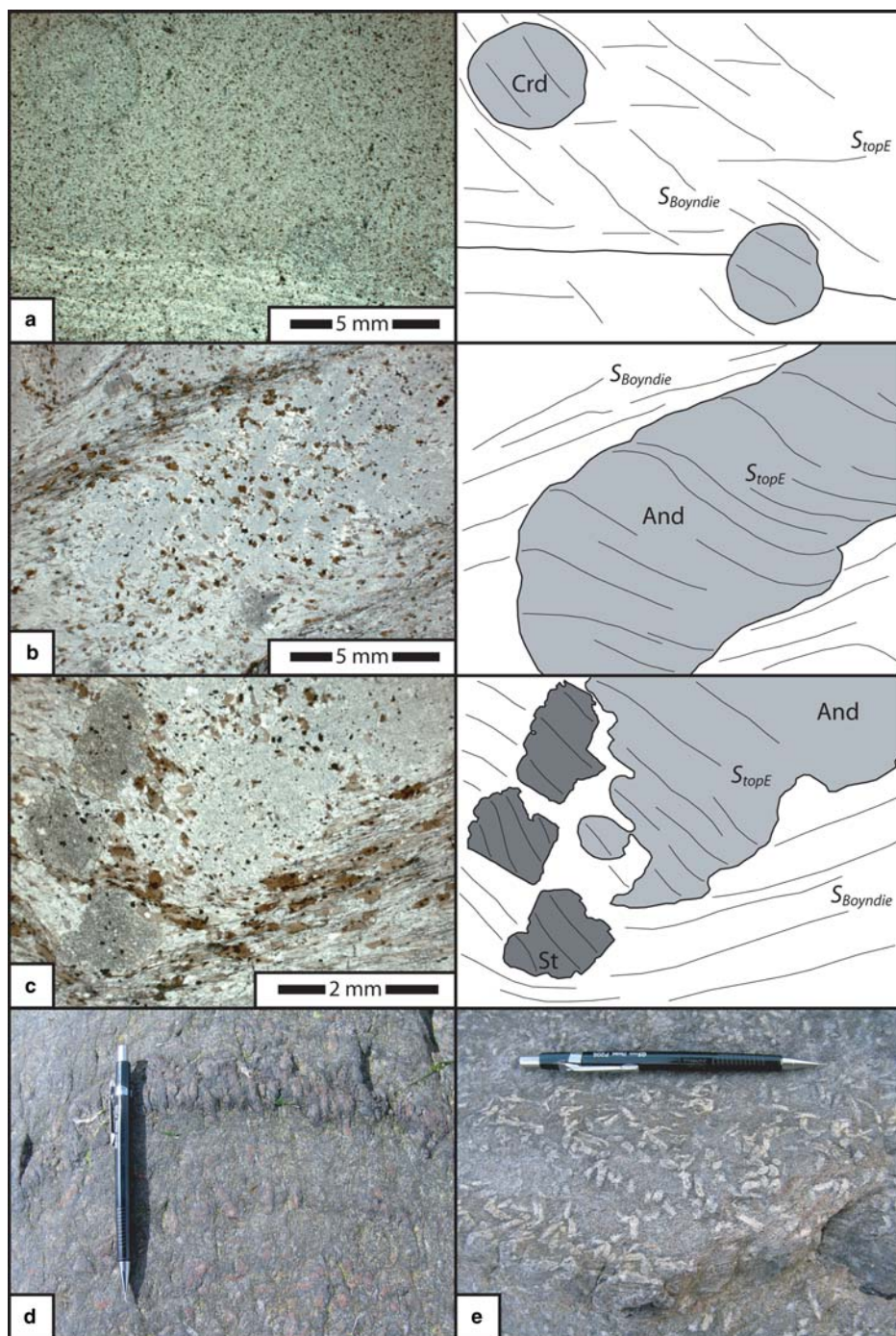
Fig. 10. Photomicrographs from the Portsoy transect displaying growth timing relationships for (**a**) a cordierite-grade semi-pelite from Banff [GPS: NJ68186455]; (**b**) an andalusite-grade semi-pelite from the west side of Boyndie Bay [GPS: NJ66626491]; (**c**) a staurolite-andalusite semi-pelite from the west side of Boyndie Bay [GPS: NJ66626491]; and field photos of (**d**) andalusite orientated in $S_{Boyndie}$ [GPS: NJ66586493, view down to the south]; and (**e**) more haphazardly orientated andalusite [GPS: NJ66276522, view down to the ESE]. Mineral abbreviations follow the recommendations of Kretz (1983).

White mica and biotite occur in both the early, included fabric and the later, high-angle fabric. Correlation between fabrics in the field and those in thin section suggests that the straight internal fabric developed during SZ_{topE} deformation and that the external fabric, that wraps porphyroblasts, developed in association with the $F_{Boyndie}$ folding. S_{topE} inclusion trails curve toward an $S_{Boyndie}$ orientation at grain edges. Relationships between fabrics and minerals in thin section suggest a syn-SZ_{topE} to early syn-$F_{Boyndie}$ timing for cordierite, andalusite and staurolite growth in the staurolite zone.

Sillimanite zone. Two discrete episodes of sillimanite growth are preserved in rocks of the Portsoy transect, which, together, form the sillimanite zone of the Buchan Block (Fig. 2a). Sillimanite that grew during a first episode is restricted to units of the Cowhythe Gneiss where it occurs in association with biotite (Johnson 1962) that grew during the early migmatization. The migmatites pre-date the intense $S_{melange}$ deformation that affected the entire Cowhythe Gneiss. U–Pb SHRIMP dating of zircon that grew during migmatization of the Cowhythe gneiss yielded an age of 1012 ± 10 Ma (G. J. H. Oliver unpublished data), indicating a pre-Grampian (Grenvillean) age for sillimanite growth within the Cowhythe Gneiss.

Sillimanite also occurs in association with gabbroic intrusions in the PSZ. The frequently-reported Portsoy Chiastolite Schist best illustrates the timing of mineral growth within the PSZ. The rock contains andalusite, kyanite and sillimanite in addition to biotite, garnet and staurolite. Chiastolite (andalusite) accumulations pre-date the main shear fabric but have been mostly replaced by kyanite (Fig. 11a). Kyanite grains are wrapped by a prominent top-to-the-east shear fabric and are dissected by associated shear bands (Fig. 11a). Inclusions within staurolite define shear bands of the reverse polarity (top-to-the-west) to those preserved within the sheared matrix (Fig. 11b) and staurolite is considered to enclose a fabric formed during a shear episode that preceded the main shearing and which accommodated movement that was opposite in polarity. Fibrolite occurs within pull-apart domains associated with boudinage of staurolite grains during the main shear deformation. Garnet grains are deformed by shear bands associated with the main shear episode. Microstructural evidence suggests that kyanite, staurolite and garnet growth occurred prior to and/or during the deformation episode that resulted in formation of the main fabric, and that sillimanite growth occurred only during the main shear deformation. Correlation with results from field mapping suggests that the dominant shear fabric within the Portsoy Chiastolite Schist is the SZ_{topE} fabric. Earlier shear bands are

correlated with the SZ_{topW1} shear episode of the regional deformation sequence.

Pelites in the PSZ commonly display an intense crenulation cleavage, which is correlated with the $F_{Boyndie}$ folding event. Staurolite and garnet from these pelites contain straight to slightly crenulated inclusion trails of white mica and quartz that are continuous with the locally dominant S_{topE} schistosity (Fig. 11c). In some samples, rotated inclusion trails are continuous with the externally dominant, top-to-the-east S_{topE} shear fabric (Fig. 11d). Staurolite and garnet from within the crenulated pelites of the PSZ appear to have grown prior to, and during the early stages of $F_{Boyndie}$ folding. Initiation of garnet growth may pre-date that of staurolite, with rotated inclusion trails (Fig. 11d) providing evidence of garnet growth during the top-to-the-east SZ_{topE} shearing.

Mylonitic units from the Portsoy Thrust zone on the east side of Links Bay contain sillimanite as elongate fibrolite felts within the dominant shear fabric. The main shear fabric wraps fibrolitic masses (Fig. 12a), suggesting that sillimanite growth occurred prior to, or in the early stages of development of the fabric. Recrystallization of white mica, biotite, plagioclase and quartz outlasted deformation associated with formation of the main fabric, as illustrated by the presence of large, recrystallized mica grains within the fabric and their association with recrystallized plagioclase and foam textures in quartz (Fig. 12a). The mylonitic fabric on the east side of Links Bay has been assigned a SZ_{topW2} structural timing. Accordingly, sillimanite growth occurred in these rocks prior to, or during the SZ_{topW2} thrusting. White mica and biotite growth outlasted deformation associated with SZ_{topW2} thrusting.

Based on cross-cutting relationships observed in thin section and correlation of microstructures with structural mapping, it appears that kyanite within the sillimanite-grade units of the PSZ probably grew pre- to syn-SZ_{topE}, whereas garnet, staurolite and sillimanite probably grew syn-SZ_{topE} and overlapped with the initial stages of $F_{Boyndie}$ folding, and possibly with SZ_{topW2} shearing. White mica and biotite is likely to have grown throughout the SZ_{topE} and $F_{Boyndie}$ (and SZ_{topW2}) deformations. The most that can be inferred concerning the timing of andalusite growth in units from within the PSZ is that it pre-dates development of the pervasive S_{topE} shear fabric and thus occurred prior to the SZ_{topE} shear episode.

Kyanite zone. Within the kyanite zone (*sensu* Hudson 1980) of the Portsoy transect, rocks that contain kyanite as the highest-grade mineral are rare. Kyanite was not found among the thin sections produced from sampling. However, the timing of
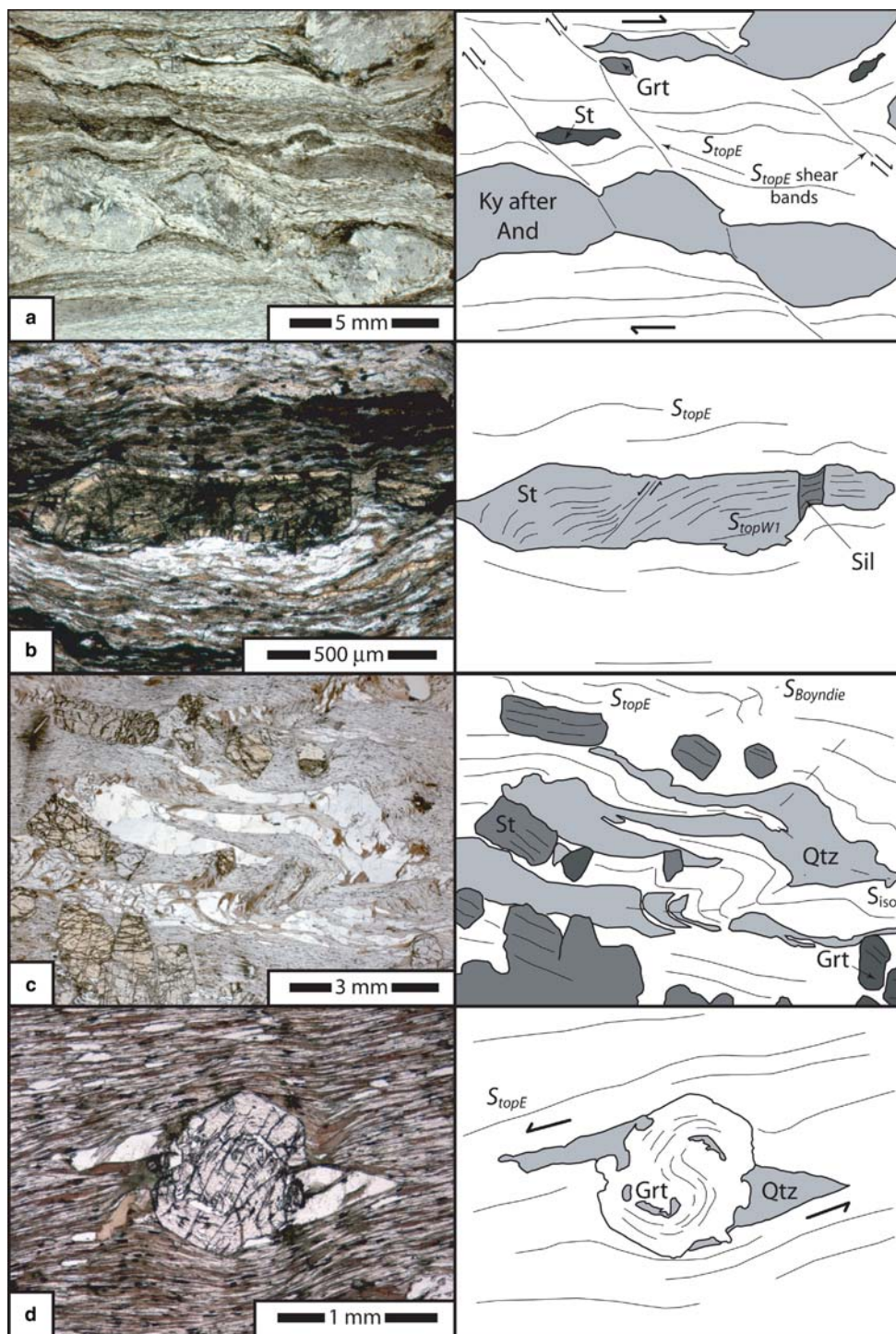
Fig. 11. Photomicrographs from the Portsoy transect displaying mineral growth/structural timing relationships for (**a**−**b**) the Portsoy Chiastolite Schist [GPS: NJ58436638]; and (**c**−**d**) a folded garnet-staurolite schist from the Portsoy Shear Zone [GPS: NJ58186650]. Mineral abbreviations follow the recommendations of Kretz (1983).
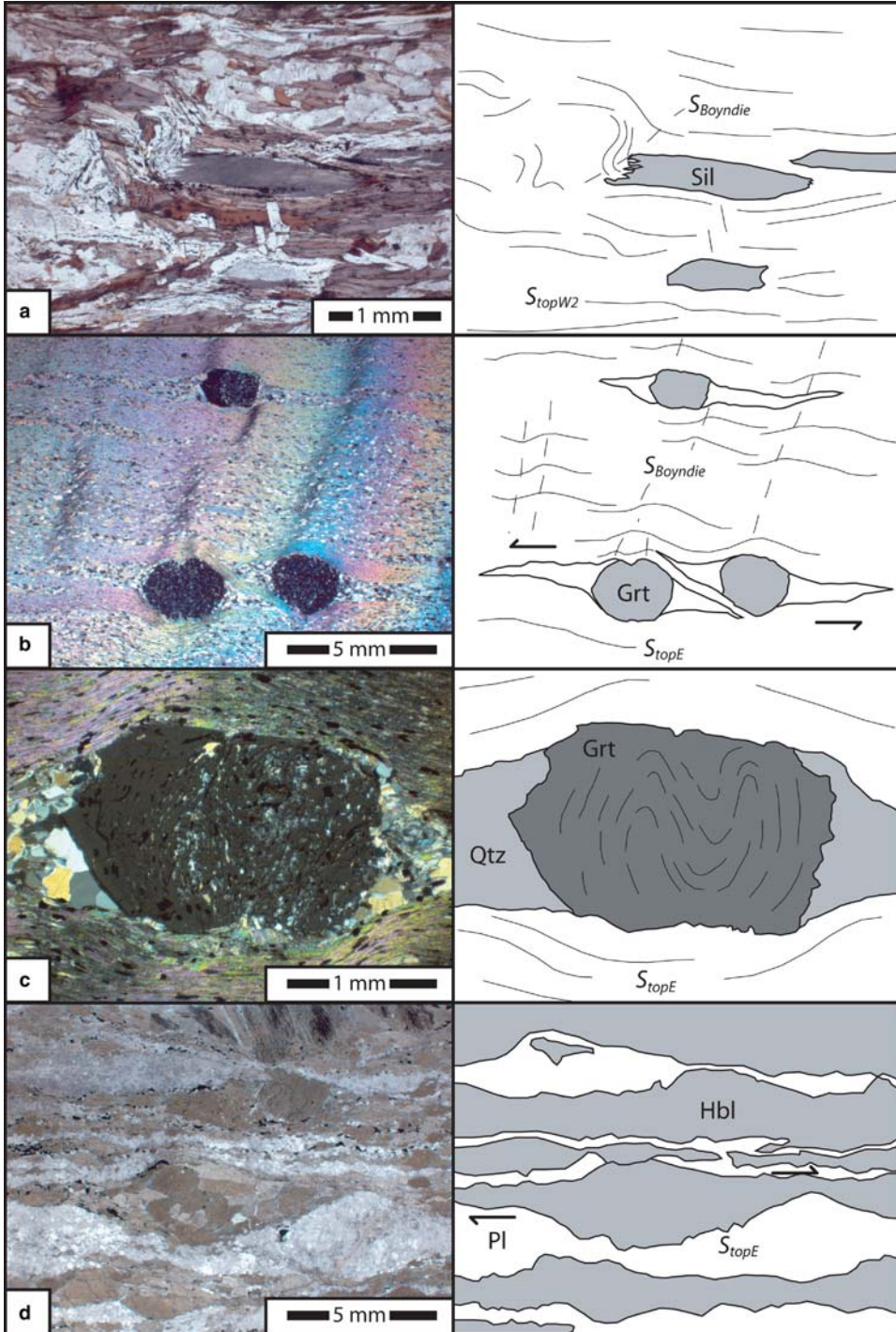
Fig. 12. Photomicrographs from the Portsoy transect displaying mineral growth/structural timing relationships for (**a**) a sillimanite-grade schist from the Portsoy Thrust [GPS: NJ59476614]; (**b–c**) a garnet schist from Logie Head [GPS: NJ53096772]; and (**d**) amphibolitized gabbro from the Portsoy Gabbro body [GPS: NJ58786637]. Mineral abbreviations follow the recommendations of Kretz (1983).

kyanite growth can be inferred from observations made in the Portsoy Chiastolite Schist, which had reached kyanite-grade conditions prior to later sillimanite growth.

A shear fabric with top-to-the-east kinematic indicators wraps garnets from the kyanite zone at Logie Head (Fig. 12b). Garnet grains contain what appear to be isoclinal folds at a high angle to the external shear fabric, defined by included fabrics that are truncated by the external fabric (Fig. 12c) but may also represent spiralled inclusions cut at an oblique angle. The high-angle, truncated internal fabric defines the apparent isoclinal folds within the garnet (Fig. 12c), suggesting growth timing synchronous with development of the inclusion trail geometries. The external shear fabric is correlated with the SZ_{topE} shearing. The isoclines in the garnet are considered to have developed either during the F_{iso} deformation, or during SZ_{topE} porphyroblast rotation. Microstructurally, garnet growth appears to have occurred during F_{iso} folding (or during SZ_{topE} if spiralled inclusion trails form the included folds), whereas kyanite growth probably occurred prior to and during SZ_{topE} shearing.

Amphibolitization of gabbros. Shear deformation in gabbros of the sillimanite-grade PSZ is defined by plagioclase and hornblende banding and includes asymmetric lozenges consistent with a top-to-the-east shear (Fig. 12d). Small grain sizes in both hornblende and plagioclase (Fig. 12d) are consistent with (re)crystallization of these minerals in a dynamic environment undergoing active deformation. Crystallization textures suggest that growth of hornblende and plagioclase was contemporaneous with formation of mylonitic fabrics. The top-to-the-east shear fabric preserved within the gabbros appears to represent SZ_{topE} deformation in these units. Amphibolitization of the gabbros most probably occurred during the SZ_{topE} shearing episode.

Summary of metamorphic microstructures

West of the PSZ on the Portsoy coastal section, garnet growth appears to have occurred during F_{iso} and into SZ_{topE} and to have partially overlapped with SZ_{topE} in the kyanite zone. In these rocks kyanite grew prior to and during SZ_{topE}. However, if included folds in garnet represent spiralled inclusion trails formed by porphyroblast rotation during the SZ_{topE} shear, then garnet within the kyanite zone grew exclusively during SZ_{topE}. Sillimanite-grade units from the PSZ experienced syn- and possibly pre-SZ_{topE} kyanite growth and growth of garnet, staurolite and sillimanite during SZ_{topE} deformation and into the initial stages of $F_{Boyndie}$ and SZ_{topW2}. To the east of the PSZ, in staurolite- and andalusite-grade units of the

Buchan Block, growth of staurolite, andalusite and cordierite occurred from syn-SZ_{topE} to early syn-$F_{Boyndie}$ times. Cordierite from the cordierite zone appears to overprint the S_{topE} fabric and probably grew entirely during $F_{Boyndie}$ folding. White mica and biotite across the transect indicate a growth timing from pre-SZ_{topE} through to post-$F_{Boyndie}$, though biotite growth in the biotite zone appears to have occurred exclusively during $F_{Boyndie}$. Growth timings are recorded for each mineral within its respective mineral zone as follows:

(a) pre- to syn-SZ_{topE} for kyanite;
(b) syn-SZ_{topE} to early syn-$F_{Boyndie}$ for sillimanite;
(c) syn-SZ_{topE} to early syn-$F_{Boyndie}$ for staurolite and andalusite, and
(d) syn-$F_{Boyndie}$ for cordierite and biotite.

Indicator mineral growth occurred structurally later in the direction of increasing metamorphic grade (eastward) within the Barrovian-type units to the west of Portsoy. Conversely, indicator mineral growth appears to have occurred structurally later in the direction of decreasing metamorphic grade (eastward) within the Barrovian-type units to the east of Portsoy. Interpretation of the microstructural timing of metamorphic growth in the Portsoy area have been combined with the tectonic sequence diagram (Table 1) to construct a crystallization sequence diagram that shows the structural timing of mineral growth associated with the Grampian-age Barrovian-type metamorphism and the Buchan metamorphism (Fig. 13).

In addition to Grampian-age growth, minerals that appear to pre-date Grampian tectonism occur on the Portsoy transect. Sillimanite within the Cowhythe Gneiss appears to be Grenvillian in age and there is no evidence to suggest that andalusite of the Portsoy Chiastolite Schist grew during Grampian times.

Magma geochemistry

Whole-rock major and trace element geochemistry was carried out on five metabasite, one felsic and seven gabbro samples collected from Portsoy and the surrounding region (Fig. 2b). On the basis of field relationships, the sample set can be split into two groups: the Dalradian metabasites (and Portsoy Granite) and the Grampian gabbros. The Dalradian metabasites and Portsoy Granite appear to have been deposited/emplaced during the $M_{Dalradian}$ magmatism, prior to the prominent regional metamorphism that affected the region. The Grampian gabbros, consisting of variably altered mafic intrusive units emplaced and crystallized during the regional metamorphism and SZ_{topE} deformation, are products of the $M_{Grampian}$ magmatic event.
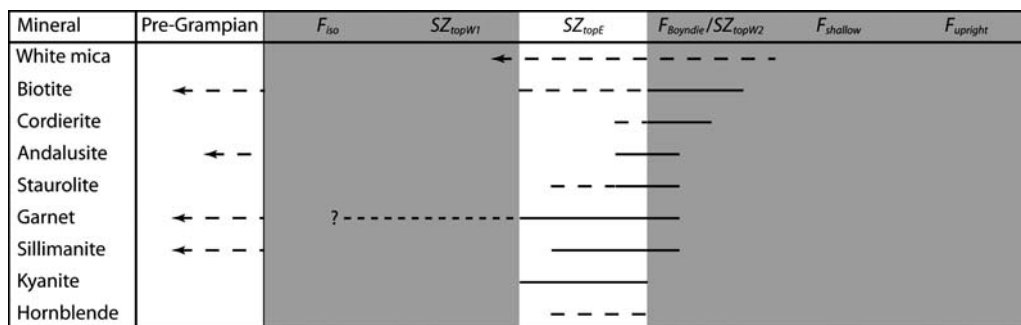
Fig. 13. Crystallization sequence diagram displaying structural timing of metamorphic mineral growth across the Portsoy transect (dashed lines). Timing of indicator mineral growth within their respective mineral zones is shown by continuous lines.

Results

The results of major element and trace element analyses carried out on the Portsoy samples are summarized in Table 2. Whole-rock geochemistry is discussed in two segments; in terms of major element systematics and trace element systematics. Implications of the whole-rock geochemistry for the petrogenesis of the magmatic suites are presented as part of the discussion section.

Major element systematics. With respect to the igneous rock classification system of Cox *et al.* (1979) samples of the Dalradian metabasites plot within the basaltic andesite and andesite fields. Sample GOPO 45, obtained from the Portsoy Granite, is alkaline granite in composition. According to grain size, alkali abundance and silica abundance, the Grampian samples are all gabbros or are intermediary in composition between gabbro and diorite.

Co-variation diagrams of major element compositions v. SiO_2 demonstrate differences in the range of major element compositions displayed by the Dalradian metabasites and the Grampian gabbros. The Dalradian metabasites display a greater range in SiO_2, Al_2O_3 and MgO than the Grampian gabbros (Fig. 14a–d). Notwithstanding some scatter in the co-variation diagrams, trends defined by the Dalradian metabasites display an inflection in Al_2O_3, FeO, MgO and TiO_2 when plotted against SiO_2 (Fig. 14a–d). In contrast, the Grampian gabbros show linear compositional trends in Al_2O_3, FeO, MgO and TiO_2 with SiO_2 (Fig. 14a–d). Co-variation diagrams that map Na_2O, K_2O and SiO_2 display less well defined trends (Fig. 14e–h).

In K_2O v. SiO_2 space, samples belonging to the Dalradian metabasites display alkaline compositions whereas those of the Grampian gabbros display sub-alkaline compositions (Fig. 14e). The opposite is the case for Na_2O v. SiO_2 space, which defines the Dalradian metabasites and Grampian gabbros as sub-alkaline and alkaline in composition, respectively (Fig. 14f). According to Middlemost's (1975) alkalinity classification system, the two populations of igneous units that crop out in the Portsoy region can each be described as transitional between alkaline and sub-alkaline in composition. In terms of total alkalis, compositions from both sample sets plot near to the alkaline/sub-alkaline transition in the basalt classification system developed by Miyashiro (1978) (Fig. 14g), though more alkaline compositions are displayed by units belonging to the Grampian gabbros. In K_2O v. Na_2O space, Dalradian metabasites display potassic compositions, whereas the Grampian gabbros display sodic compositions (Fig. 14h). The Dalradian metabasites belong to the high potassium, 'Potash series' of Middlemost (1975), whereas the same classification system defines the Grampian gabbros of Portsoy as members of the 'Sodic series' (Fig. 14h).

Trace element systematics. Trace element compositions for the Dalradian metabasites and Grampian gabbros are expressed with respect to the average Normal Mid Ocean Ridge Basalt (N-MORB) composition (Sun & McDonough 1989) in the form of a Rare Earth Element (REE) plot (Fig. 15a) and an extended trace element plot (Fig. 15b). Each of the plots of Figure 16 displays, from left to right, abundance ratios (against N-MORB) for trace elements that are decreasingly compatible in mantle melts.

On the N-MORB normalized REE plot of Figure 15a, all samples show a slope across the Heavy Rare Earth Elements (HREEs) (Gd/Yb > 1) and are enriched in the Light Rare Earth Elements (LREEs) with respect to the HREEs. Samples of the Dalradian metabasites display a

Table 2. *Major- and trace-element data from igneous units surrounding Portsoy*

	Dalradian metabasites and granites						Grampian gabbros						
Sample	GOPO 33	GOPO 38	GOPO 41	GOPO 42	GOPO 43	GOPO 45	GOPO 26	GOPO 27	GOPO 28	GOPO 30	GOPO 35	GOPO 39	GOPO 40
GPS	[NJ59196645]	[NJ58226645]	[NJ55506700]	[NJ55506700]	[NJ58976642]	[NJ57506520]	[NJ59116647]	[NJ58766635]	[NJ58766635]	[NJ58886639]	[NJ58526640]	[NJ62906600]	[NJ63006590]
Major elements (wt%)													
SiO_2	54.52	57.10	52.09	52.49	61.42	71.87	52.56	47.87	50.53	56.18	52.71	47.59	47.93
TiO_2	0.91	0.88	0.52	0.42	1.27	0.43	1.04	1.66	1.48	1.42	2.14	2.26	2.30
Al_2O_3	15.49	20.33	9.76	9.11	16.33	14.30	17.28	15.94	15.95	14.72	15.91	14.91	15.27
$Fe_2O_3^T$	7.44	8.01	3.84	3.65	7.62	1.65	8.43	11.01	10.23	7.43	10.53	12.55	12.54
MnO	0.15	0.06	0.07	0.07	0.09	0.02	0.13	0.16	0.16	0.13	0.12	0.15	0.16
MgO	6.99	3.75	17.60	16.96	2.23	0.83	5.16	6.73	6.18	5.55	5.21	7.04	6.19
CaO	7.91	0.32	8.40	8.42	3.06	1.40	7.80	9.13	8.33	5.43	6.89	9.82	10.83
Na_2O	2.66	0.49	0.62	0.67	2.78	3.50	5.11	3.50	3.86	3.30	4.57	2.92	2.75
K_2O	1.28	3.15	2.27	2.31	3.20	4.74	0.94	0.74	1.17	1.99	0.19	0.25	0.31
P_2O_5	0.19	0.20	0.22	0.19	0.37	0.17	0.17	0.28	0.24	0.30	0.44	0.35	0.34
Cs	1.52	3.90	3.93	4.68	3.12	2.26	0.31	0.59	0.45	1.64	0.16	0.33	0.51
Rb	33.27	101.7	80.68	87.00	98.01	133.5	12.46	13.03	18.18	41.27	1.85	4.36	4.16
Ba	208.3	413.1	257.7	332.5	706.7	863.0	143.4	129.7	182.4	342.0	42.52	77.12	113.2
Th	1.46	15.02	7.65	7.43	12.18	11.24	0.76	1.25	1.34	1.81	0.63	0.71	0.71
U	0.90	3.11	1.13	1.01	1.06	4.40	0.38	0.47	0.50	0.87	0.19	0.19	0.19
Nb	5.79	17.19	9.86	6.27	19.04	6.13	12.95	14.76	13.39	17.43	24.73	10.11	10.08
Ta	0.57	1.36	0.73	0.63	1.10	1.16	2.40	0.88	0.93	1.25	1.77	0.84	0.81
Pb	10.11	13.09	9.29	11.23	21.23	17.26	6.72	4.87	5.09	10.94	6.27	10.80	3.57
Sr	217.6	10.42	73.91	76.00	158.8	129.8	274.3	221.1	232.5	219.9	338.7	332.4	288.3
Zr	26.78	129.6	88.74	75.75	46.65	494.1	33.95	52.01	38.41	42.44	16.36	24.76	17.41
Hf	0.70	3.80	2.42	2.20	1.22	2.06	0.98	1.43	1.15	1.07	0.49	0.87	0.72
Y	15.77	25.94	19.53	16.26	25.97	19.89	20.53	25.00	23.53	21.79	26.13	25.42	25.13
V	149.4	63.11	40.13	38.25	73.46	15.40	118.3	164.8	164.7	139.3	157.1	184.2	181.0
Cu	27.93	25.39	12.00	3.53	19.87	0.13	36.52	33.07	29.08	25.70	15.20	53.48	39.67
Zn	88.52	61.60	76.47	53.78	80.28	17.21	61.62	79.83	95.45	55.72	54.58	96.21	91.08
Ni	43.95	68.60	50.85	10.77	12.94	2.90	118.9	37.41	50.12	41.70	24.40	99.37	82.45
Cr	207.8	69.90	69.62	58.89	43.52	15.94	131.4	167.2	135.5	78.75	125.8	138.7	130.5

(*Continued*)

Table 2. *Continued*

	Dalradian metabasites and granites						Grampian gabbros						
Sample	GOPO 33	GOPO 38	GOPO 41	GOPO 42	GOPO 43	GOPO 45	GOPO 26	GOPO 27	GOPO 28	GOPO 30	GOPO 35	GOPO 39	GOPO 40
GPS	[NJ59196645]	[NJ58226645]	[NJ55506700]	[NJ55506700]	[NJ58976642]	[NJ57506520]	[NJ59116647]	[NJ58766635]	[NJ58766635]	[NJ58886639]	[NJ58526640]	[NJ62906600]	[NJ63006590]
Trace elements (ppm)													
La	12.89	43.45	21.18	20.58	46.20	26.47	10.01	14.41	13.16	19.73	21.40	9.02	8.81
Ce	26.82	92.23	44.94	43.55	95.97	58.17	22.15	35.11	31.41	42.03	46.45	22.58	22.44
Pr	3.23	10.87	5.57	5.32	11.80	7.21	2.82	4.65	4.17	5.07	6.06	3.36	3.39
Nd	12.68	39.94	20.16	19.11	44.82	26.15	12.05	19.22	17.56	20.01	24.70	16.27	16.27
Sm	2.70	7.11	3.68	3.57	8.35	5.48	2.97	4.38	4.02	4.06	5.49	4.64	4.68
Eu	1.19	1.50	0.90	0.84	1.93	1.11	1.16	1.34	1.27	1.49	1.91	1.85	1.83
Gd	2.84	6.83	3.99	3.63	8.08	5.32	3.37	4.71	4.51	4.38	5.87	5.15	5.28
Tb	0.44	0.92	0.57	0.50	1.07	0.75	0.58	0.73	0.70	0.65	0.88	0.83	0.84
Dy	2.65	4.87	3.25	2.81	5.41	3.88	3.41	4.19	4.06	3.74	4.71	4.52	4.56
Ho	0.56	0.99	0.69	0.58	1.03	0.70	0.78	0.88	0.85	0.81	0.93	0.94	0.94
Er	1.50	2.57	1.85	1.52	2.40	1.70	2.06	2.38	2.19	2.08	2.29	2.34	2.30
Tm	0.22	0.38	0.26	0.24	0.33	0.24	0.31	0.32	0.32	0.31	0.31	0.32	0.31
Yb	1.50	2.56	1.74	1.57	2.06	1.63	1.96	2.13	2.18	2.09	1.99	2.03	1.94
Lu	0.23	0.37	0.26	0.23	0.29	0.23	0.28	0.31	0.31	0.31	0.28	0.27	0.27
Nb/La	0.45	0.40	0.47	0.30	0.41	0.23	1.29	1.02	1.02	0.88	1.16	1.12	1.14
Ba/Rb	6.3	4.1	3.2	3.8	7.2	6.5	11.5	10.0	10.0	8.3	23.0	17.7	27.2
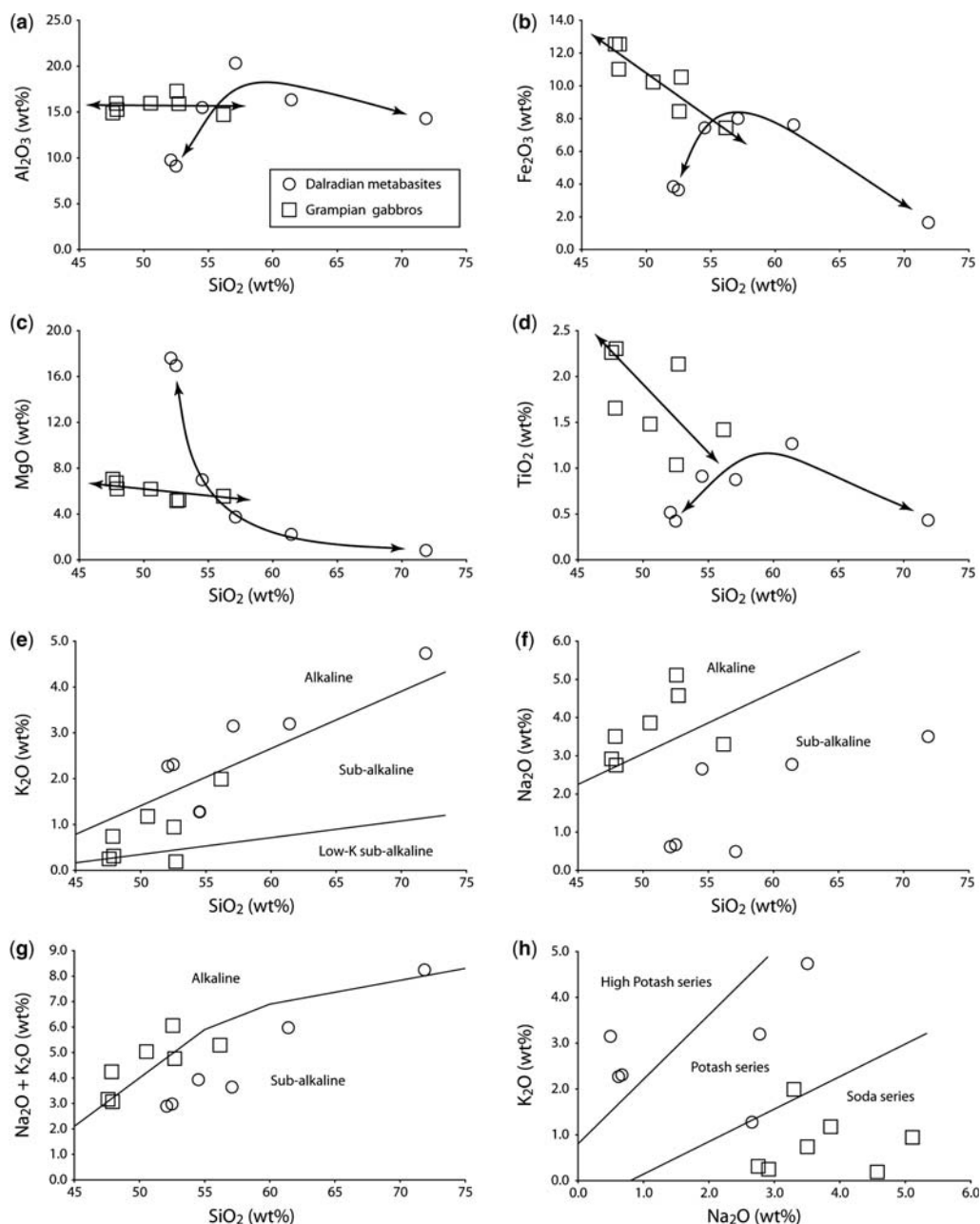
Fig. 14. Covariation diagrams for igneous rock samples from the Portsoy region displaying concentration of (**a–d**) some major oxides v. SiO_2; (**e**) K_2O v. SiO_2; (**f**) Na_2O v. SiO_2; (**g**) total alkalis v. SiO_2; and (**h**) K_2O v. Na_2O. Fields used for alkaline v. sub-alkaline classification (Miyashiro 1978) are shown on Figure 14e–g and the different alkaline classification fields of Middlemost (1975) are shown on Figure 14h. Legend for Figure 14a is applicable to all figures.

more significant gradient across the REEs than those of the Grampian gabbros and carry a slightly negative Eu anomaly that does not appear in the Grampian gabbro REE plots (Fig. 15a). For both the Dalradian metabasites and the Grampian gabbros, a decrease in the slope of the REE plot occurs with decreasing compatibility (Er, Tm, Yb and Lu all occur at values near to unity), resulting in
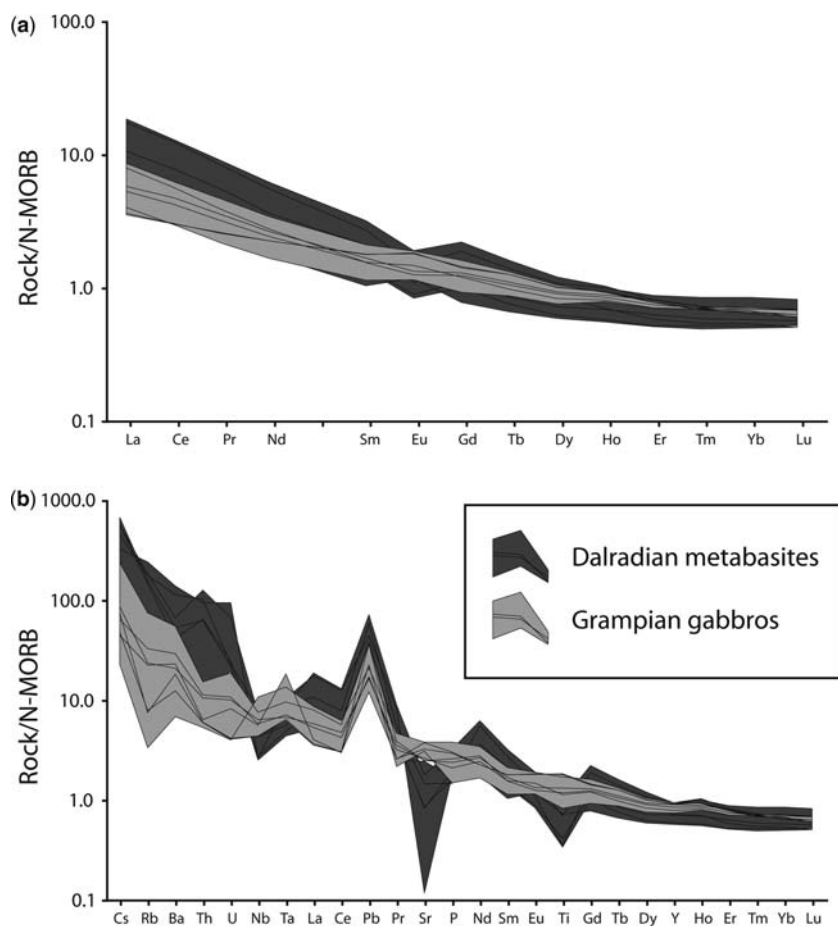
Fig. 15. (**a**) N-MORB-normalized REE; and (**b**) trace element plots for igneous rock samples from the Portsoy region. Legend for Figure b can be applied to Figure a.

upwards concavity of the plot in the region of the HREEs (Fig. 15a).

Samples taken from both the Dalradian metabasites and Grampian gabbros display marked enrichments in the LILEs (e.g. Cs, Rb, Ba, Th, U and Pb) with respect to the REEs, being generally 10–1000 times higher than values expected for N-MORB (Fig. 15b). Similar to the LREEs, enrichments in the LILEs are more pronounced for the Dalradian metabasites than for the Grampian gabbros (Figs 15b & 16a, b). The Dalradian metabasites also display a significant depletion in Sr that is not seen in trace element plots for the Grampian gabbros (Fig. 15b).

With regard to the HFSEs, inspection of Figure 15b reveals depletion in Nb and Ta relative to neighbouring REEs such as La and Ce for samples of the Dalradian metabasites, but no such depletion for samples of the Grampian gabbros. In addition, significant depletion in Ti is apparent for the Dalradian metabasites but not for the Grampian gabbros (Fig. 15b). An instructive measure of HFSE depletion/enrichment is Nb abundance relative to that of La. Markedly higher values of Nb/La were obtained from analyses carried out on the Grampian gabbros in comparison to those carried out on samples of the Dalradian metabasites. The Nb/La v. SiO_2 plot of Figure 16c demonstrates a clear distinction between the two populations on the basis of differing Nb/La values for similar SiO_2 and defines a trend toward decreasing Nb/La with increasing SiO_2 for each of the sample sets. In Nb/La v. Ba/Rb space, samples of the Dalradian metabasites are positioned separately from samples of the Grampian gabbros, the latter plotting at Nb/La values of close to unity and at higher Nb/La
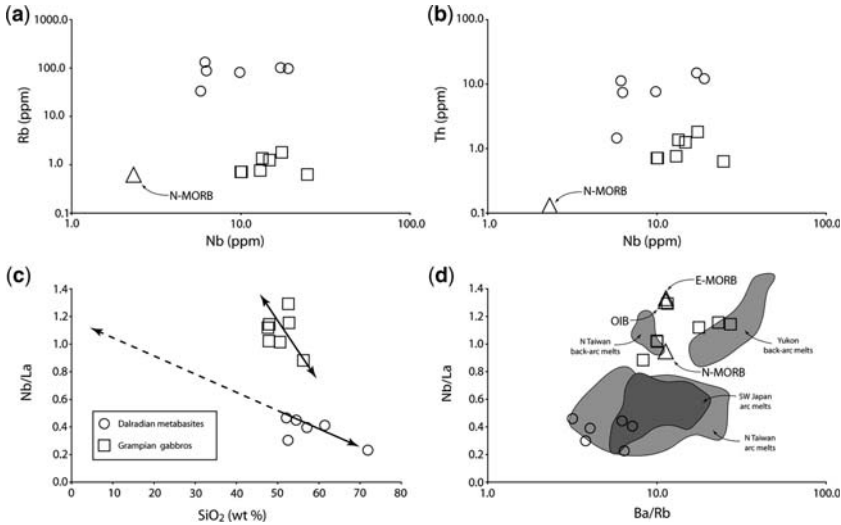
Fig. 16. (**a**) Th v. Nb; (**b**) Rb v. Nb; (**c**) Nb/La v. SiO$_2$; and (**d**) Nb/La v. Ba/Rb plots for igneous samples from the Portsoy region. Figure 16d displays fields for some previously characterized mafic magma suites. Legend for Figure 14c can be applied to all figures. North Taiwan, SW Japan and Yukon data from Wang *et al.* (1999), Piercey *et al.* (2002) and Uto *et al.* (2004), respectively.

and Ba/Rb values than the former (Fig. 16d). Zircon fractionation related to incomplete digestion following acid dissolution techniques used to prepare the analysed samples is responsible for depletion in Zr and Hf relative to other HFSE. Zr and Hf results were deliberately omitted from Figure 15b to avoid assignation of undue relevance to global depletions in these elements.

Discussion

Examination of the tectonic sequence diagram for the Portsoy transect (Table 1) reveals details of the tectonic evolution of the Grampian Terrane. An evolution in movement sense across the Portsoy-Duchray Hill Lineament (PDHL), from top-to-the-west (SZ_{topW1}) to top-to-the-east (SZ_{topE}) to top-to-the-west (SZ_{topW2}) is apparent (Table 1). Top-to-the-east movement (SZ_{topE}) occurred during mantle melting ($M_{Grampian}$) and sediment deposition at the top of the Dalradian Supergroup ($B_{Grampian}$). Metamorphism in the Barrovian-type units was synchronous with SZ_{topE}, whereas that in the PDHL and the Buchan Block began during SZ_{topE} shearing and continued into the subsequent folding ($F_{Boyndie}$) and top-to-the-west shear episode (SZ_{topW2}) (Fig. 13). Being of lower pressure but identical (initial) structural age, metamorphism of the Buchan Block with respect to the Barrovian-type units to its west can be used to suggest that the Buchan Block and Barrovian-type units to the

west formed the hanging wall and footwall of the PDHL, respectively, at this time. Similar depths of emplacement for members of the Grampian gabbros, calculated from contact metamorphic assemblages in the Dalradian country rock (Droop & Charnley 1985), suggest that the shear zones of Ashcroft *et al.* (1984), into which they were emplaced, formed a sub-horizontal sheet, consistent with gentle dips for the shear zones during SZ_{topE} deformation. The metamorphic pattern across the PDHL (higher-pressure units to the west and lower-pressure units to the east) is consistent with metamorphism and crustal heating during top-to-the-east, normal-sense shear movement on the low-angle shear zones that comprised the PDHL of SZ_{topE} times. Shear planes within the PDHL must have dipped gently toward the east or SE, suggesting that the SZ_{topE} episode accommodated crustal extension. Episodes of top-to-the-west shearing represent phases of thrusting across the PDHL, and vertical thickening of the Grampian Terrane. An evolution in deformation style during the Grampian orogenic episode from shortening ($F_{iso}SZ_{topW1}$), to extension (SZ_{topE}), to renewed shortening ($F_{Boyndie}SZ_{topW2}$) is apparent in the tectonic sequence diagram of Table 1. The hanging wall (Buchan Block) appears to have been thrust westward over the footwall (Barrovian-type units) during SZ_{topW1}, and again during SZ_{topW2}, with unroofing of the Barrovian-type units (SZ_{topE}) occurring between the thrusting episodes.

The origin of the Dalradian and Grampian magmas

The compositional differences between the Dalradian metabasites and the Grampian gabbros suggest that their petrogenesis was distinct. A significant range in major element composition for the Dalaradian igneous units (Fig. 14a–d) is consistent with fractionation during crystallization. Crystallization then removal of cumulus plagioclase from the system can account for the negative Eu (Fig. 15a) and Sr (Fig. 15b) anomalies displayed by the sample set. The more limited range in Grampian gabbro major element compositions (Fig. 14a–d) is suggestive of less pronounced fractionation. Scatter in alkalis (Fig. 14e, f) with respect to the other major elements (Fig. 14a–d) suggests that the alkali species (e.g. Na_2O and K_2O) were mobilized following crystallization. The Dalradian metabasites and Grampian gabbros display compositions that are transitional between alkaline and sub-alkaline, and are potassic and sodic, respectively. However, the apparent mobilization of Na_2O and K_2O makes perilous any attempt to relate rock type (as defined by alkali abundance) to melt origin or tectonic setting.

Negative gradients in the REEs for the Dalradian metabasites and the Grampian gabbros (Fig. 15a) are likely to have an origin in fractionation by partial melting of the source region. At low degrees of partial melting, garnet lherzolite mantle will produce magmas that display large gradients across the HREEs, related to sequestration of the heavier elements in restitic garnet (cf. Kay & Gast 1973). Relatively flat HREE patterns for the Dalradian metabasites and the Grampian gabbros (Fig. 15a) are consistent with partial melting (for the most part) at mantle depths more shallow than the spinel lherzolite–garnet lherzolite transition (i.e. pressures <18 to 27 kbar for temperatures of 1100–1500 °C: O'Neill 1981; Klemme & O'Neill 2000). Mantle & Collins (2008) determined an exponential relationship between maximum Ce/Y ratios recorded in basalts from active arc volcanos and the seismically defined Moho depth beneath them. Maximum Ce/Y ratios of 3.70 and 1.93 for the Dalradian metabasites and Grampian gabbros, respectively, correspond to crustal thicknesses of about 45 km during Dalradian magmatism and about 33 km during Grampian magmatism, according to the Mantle & Collins (2008) relationship. These values suggest that the crust was thinner during Grampian (syn-orogenic) magmatism than it was during Dalradian (possibly rift-related) magmatism.

LILE enrichments are apparent in the geochemistry of both the Dalradian metabasites and Grampian gabbros from Portsoy (Fig. 15b) and are associated with considerable assimilation of crustal material during ascent and emplacement of the magmas, or possibly with their derivation from a mantle source contaminated with a LILE-rich fluid or magma component.

Nb/La and Ba/Rb compositions for the Grampian gabbros plot near to N-MORB, E-MORB and OIB compositions (Sun & McDonough 1989) and, in Nb/La v. Ba/Rb space, overlap with decompression melting fields defined by basalts erupted during post-collisional extension in northern Taiwan (Wang *et al.* 1999) and back-arc extension in the Yukon (Piercey *et al.* 2002; Fig. 16d). Units of the Dalradian metabasites plot at significantly lower Nb/La and Ba/Rb and, in Nb/La v. Ba/Rb space, overlap with syn-collisional arc basalts from northern Taiwan (Wang *et al.* 1999) and SW Japan (Uto *et al.* 2004; Fig. 16d). In mantle melts, depletion in HFSEs relative to N-MORB can represent a primary melt feature (e.g. Pearce 1983; Kelemen *et al.* 1990; Saunders *et al.* 1991) or may be the result of assimilation of continental crust – for which quoted typical Nb/La values range from 0.35 (Condie 1993) to 0.83 (Rudnick & Fountain 1995), in comparison to 0.93 for N-MORB (Sun & McDonough 1989). It is conceivable that trends in the individual sample populations of Figure 16c represent the effects of varying influence of crustal assimilation on Nb/La ratios, with decreasing Nb/La and increasing SiO_2 representing an increasing HFSE-depleted continental crust component in the magmas. However, extrapolation of Nb/La values back to that for N-MORB yields SiO_2 concentrations for the Dalradian metabasites of around 20 wt% (Fig. 16c), an unrealistically low figure for silicate melts. It appears that HFSE depletions observed for the Dalradian metabasites did not occur solely as the result of crustal assimilation. The melts that produced the Dalradian metabasites and Grampian gabbros originated in the same region of the sub-Grampian asthenosphere, and differing HFSE abundances are unlikely to have been inherited from the melt source region. Consequently, the origin of differing HFSE signatures for the two sample sets must lie in different melting processes. HFSE depletions are a ubiquitous geochemical signature in arc settings where mantle melting is assisted by fluid fluxing of the mantle wedge. The HFSE abundances displayed by the Dalradian metabasites are consistent with melting of a HFSE-fertile asthenosphere in the presence of fluids, whereas the Grampian gabbros appear to have derived from decompression melting of the same source, in the absence of fluids. The observation of similar enrichments in Rb (fluid mobile) and Th (fluid mobile only at magmatic temperatures) with respect to Nb in the Dalradian metabasites (Fig. 16a, b) provides additional evidence in support of the presence of fluids at magmatic temperatures during the Dalradian melting episode.

The geochemistry of the Dalradian metabasites indicates that their parental magmas were the product of fluid-present melting of the mantle wedge, perhaps during active subduction at c. 600 Ma. Tanner et $al.$ (2006), on the basis of geochemical and isotopic work carried out on the Dalradian granites, suggested that the Dalradian granites were A-type and thus were intruded during crustal rifting and continental breakup. A-type granites can occur in association with crustal rifting and active subduction (rather than continental breakup) (e.g. Landenberger & Collins 1996; Zhou & Li 2000). The classification of the Dalradian granites as A-type does not preclude their production above an active subduction zone. The later (c. 471 Ma) Grampian gabbros have their origins in decompression melting of the asthenosphere. For both cases, melting occurred within the spinel lherzolite field and thus beneath a lithospheric section less than about 70 km in thickness (assuming temperature at the base of the lithosphere is 1350 °C and average lithospheric density is $3\,g\,cm^{-3}$). Similar arc magmas and decompression-related magmas of differing age coexist in a number of locations that have experienced continental convergence, including the Aleutian Arc (Singer & Myers 1990), northern Taiwan (Wang et $al.$ 1999), western Ireland (Draut & Clift 2001), the Yukon (Piercey et $al.$ 2002), SW Japan (Uto et $al.$ 2004), the Carpathian-Pannonian region (Seghedi et $al.$ 2004) and western Anatolia and the Aegean (Agostini et $al.$ 2007).

A new model for Grampian orogenesis

Lithospheric-scale extension during SZ_{topE} can account for thinning of the lithosphere responsible for decompression melting of the mantle beneath the Grampian Terrane and production and emplacement the Grampian gabbros ($M_{Grampian}$). The Grampian granites may relate to melting of the lower to middle crust following emplacement of the Grampian gabbros. On the basis of Grampian gabbro whole-rock geochemistry, the base of the lithosphere during syn-orogenic mantle melting occurred at depths of less than 70 km. A less than 70 km thick

lithospheric section suggests that the lithosphere had been attenuated, even in comparison to stable continental crust, and that tectonic boundary forces, not simply gravity, drove extensional collapse of orogenic crust. Syn-deformational (SZ_{topE} age) subsidence and sediment deposition ($B_{Grampian}$) represent an expected outcome for tectonism involving significant lithospheric thinning.

During the SZ_{topE} extension, the PDHL acted as an additional heat source for both the Barrovian-type metamorphism and the Buchan metamorphism, concentrating both heat produced internally by mechanical work within the high-strain zone, and heat advected from the mantle in the form of Grampian-age mantle melts. Metamorphic mineral growth in the hanging wall and shear zone persisted into the subsequent thickening episode, which involved penetrative folding ($F_{Boyndie}$) and thrusting across the PDHL (SZ_{topW2}). Thickening of the lithosphere during $F_{Boyndie}$ and SZ_{topW2} would have terminated decompression-related mantle melting: shortening, in effect, cut off the heat supply. This process has been observed in the Lachlan Fold Belt of southeastern Australia (cf. Richards & Collins 2004). Metamorphism within the PDHL and in the hanging wall during the early stages of shortening ($F_{Boyndie}$ and SZ_{topW2}) was likely to have been related to the time required to shed heat that had concentrated in the middle crust during the preceding extension (SZ_{topE}). Thickening of the lithospheric section during $F_{iso}SZ_{topW1}$, prior to SZ_{topE}, meant that metamorphic heating was initially imparted on an overthickened crustal section and can account for the production of the higher-pressure (kyanite-grade) assemblages early in the extensional episode. Conductive dissipation of heat from the sillimanite zone can account for changes in the structural timing of peak metamorphism with decreasing metamorphic grade in the hanging wall (Buchan Block) (Fig. 13).

Movement across the PDHL juxtaposed the hanging wall against the region of maximum thinning (and maximum heating) in the footwall (Fig. 17). Regions of the footwall that had experienced heating were cooled as they moved away
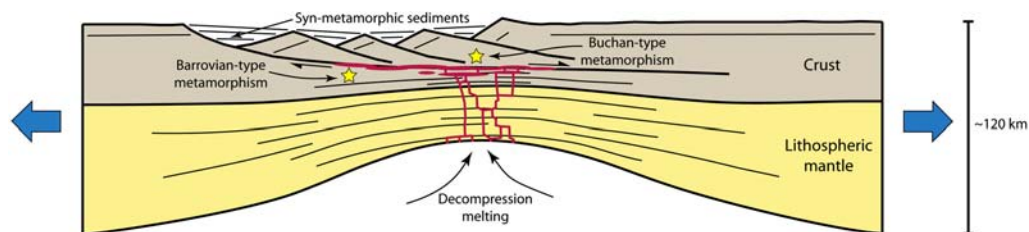
Fig. 17. Schematic diagram illustrating the hanging wall-footwall model for production of neighbouring Barrovian- and Buchan-type units during lithospheric-scale extension and decompression melting.

from the hot zone. The Buchan Block marks the current-day location of the site of lithospheric thinning during the Grampian-age extensional phase, as the high gravitational response given by the region (Fig. 4) would attest. The PDHL acted as a mid-crustal dislocation that allowed independent thermal development of Barrovian-type units and the Buchan Block. The essential aspects of the new model include a phase of extensional deformation during the Grampian orogenic episode. The pertinent features of the model are as follows:

(a) early-Grampian deformation ($F_{iso}SZ_{topW1}$) resulted in crustal thickening and produced a thick crustal section capable of producing kyanite when heated;

(b) a mid-crustal shear zone (the PDHL) separated a hanging wall (Buchan Block) from a footwall during the Grampian orogenesis;

(c) decompression melting and production of the Grampian gabbros ($M_{Grampian}$) occurred during syn-orogenic, extension-driven collapse of the orogenic edifice during SZ_{topE}, contemporaneous with deposition of the uppermost sediments of the Dalradian Supergroup;

(d) attenuation of isotherms and mechanical work during SZ_{topE} extension, coupled with advection of heat from the mantle by $M_{Grampian}$ magmatism, gave rise to the regional metamorphism (recorded in the Barrovian- and Buchan-type metamorphic units of the Grampian Terrane);

(e) independent thermal histories recorded in the hanging wall and footwall of the PDHL are related to their position with respect to the zone of maximum lower crustal heating; and

(f) the metamorphic heat supply was terminated by renewed thickening ($F_{Boyndie}SZ_{topW2}$). Overlap of metamorphism with shortening within the PDHL and in the hanging wall was related to the time required for the crust to shed heat accumulated within the highest-grade zones during SZ_{topE}.

The new model for metamorphism of the Buchan Block and Barrovian-type units to the west departs from models previously offered for the Grampian-age tectonic development of the region, which have all proposed thrusting of the Buchan Block over the Barrovian-type units during the regional metamorphism (cf. Baker 1987; Beddoe-Stephens 1990; Dempster *et al.* 1995). Past tectonic models have focused on the growth of kyanite after andalusite and its implications for pressure evolution in the footwall to the PDHL, yet largely overlooked a need to place metamorphic observations in a structural context. If one accepts that there were two generations of andalusite growth, metamorphic observations can be reconciled with evidence in the

structural and magmatic record for extension during metamorphism.

Pre-Grampian andalusite growth in the Grampian Terrane. Andalusite within the contact aureole of the Ben Vuirich Granite has been related to a thermal regime that pre-dates the Grampian event (Ahmed-Said & Tanner 2000). Although the metamorphism occurred in response to granite emplacement, it preserves a record of pressure and temperature (600 °C at ≤2 kbar) suggestive of high crustal heat flow. Early andalusite to the west of the PDHL (Chinner & Heseltine 1979; Chinner 1980) may represent heating of the upper crust during Dalradian magmatism at *c.* 600 Ma. Zenk & Schulz (2004) carried out Ca-amphibole geothermobarometry on the Green Beds of the Dalradian metabasites to demonstrate increasing pressure during the Barrovian metamorphism in Perthshire. The white mica geochemistry of units from the Barrovian metamorphic series is consistent with a pressure decrease during Barrovian metamorphic heating in Scotland in conflict with the conclusions of Zenk & Schulz (2004) (D. R. Viete unpublished data). Zenk & Schulz (2004) failed to match zoning in Ca-amphiboles with fabrics developed during the Grampian orogenic episode, making the timing of the heating recorded within their Ca-amphiboles equivocal. It is plausible that the Ca-amphibole geothermobarometry of Zenk & Schulz (2004) provides a record of steepening of the apparent crustal geotherm, from that of Dalradian-magmatic and pre-Grampian times to that during the initial thickening associated with Grampian orogenesis. Decompression during the heating associated with the regional (Barrovian- and Buchan-type) metamorphism would have followed.

Age of the gneissic units and the role of the PDHL. On the basis of Rb–Sr geochronology and structural geology, Sturt *et al.* (1977) and Ramsay & Sturt (1979) proposed that some of the gneisses that crop out in association with high-strain zones of the Buchan Block formed prior to the Grampian orogenic episode. Mapping carried out on the migmatitic units of the Aberdeenshire coast between Logie Head and Macduff (Durnhill Quartzite and Cowhythe Gneiss) yielded results consistent with pre-Grampian migmatization (Table 1), and thus supports the position taken by Sturt *et al.* (1977) and Ramsay & Sturt (1979). Leucosome from migmatites of the Cowhythe Gneiss contains 1012 ± 10 Ma (U–Pb SHRIMP) zircon overgrowths (G. J. H. Oliver unpublished data). The Cowhythe Gneiss is thought to represent Grenvillean basement to the Dalradian. So, how could it be that thin slices of basement found themselves caught up in the sequence they originally floored?

The Cowhythe Gneiss is bounded, to its east and west, by high-strain zones that preserve opposing movement sense. On its east side, the SZ_{topE}-age Boyne Line of Read (1955) separates the Cowhythe Gneiss from the Boyne Limestone, and on its west side, the SZ_{topW2}-age Portsoy Thrust of Elles (1931) separates it from the Grampian gabbros that intruded the Portsoy Group. Like the Cowhythe Gneiss, the Durnhill Quartzite is bounded on both sides by sheared units that display different senses of movement (SZ_{topE} shear zone on the west and SZ_{topW1} shear zone on the east) (Fig. 6). In each case, basement and Dalradian units may have been juxtaposed following the earlier shear movement, with later, opposite-sense movements on the opposing side responsible for abandonment of the basement slice.

Shear zones are not perfectly planar features, they anastomose and, along their length, can fork and merge. Reactivation of a broad zone of shear, associated with a switch in deformation mode (from extension to shortening or vice versa), will not necessarily exploit the same internal shear zones as were utilized during earlier deformation. Accordingly, lenses of pseudo-exotic material can be stranded as the block from which they were sourced returns to the region whence it came. Repeated reactivation of the PDHL under different tectonic regimes can account for the presence of basement slices within the lithostratigraphy. The tectonic sequence diagram of Table 1 demonstrates shear zone reactivation in the $SZ_{topW1}SZ_{topE}$ ... SZ_{topW2} sequence it displays. Major shear zones that have accommodated movements across one or more deformation mode switches have been termed 'shuffle zones' (Beltrando *et al.* 2007, 2008; Forster & Lister 2009). Interleaving of units of different affinities, that record different tectonic histories, represents a fundamental feature of shuffle zones (Beltrando *et al.* 2007, 2008; Forster & Lister 2009). The PDHL offers a perfect candidate for a mid-crustal, Grampian-age shuffle zone.

Age of deposition for the uppermost Dalradian. An additional stratigraphic concern that arises with the proposal of the syn-Grampian extension model is the depositional age of the uppermost units of the Dalradian (the Whitehills and Boyndie Bay Groups and the Macduff Slates). Downie *et al.* (1971) gave the Macduff slates a tentative Arenig (*c*. 479–466 Ma: Cooper & Sadler 2004) age based on the presence of metamorphosed microfossil fragments that resembled known species of chitonozoa. The chitonozoans they identified included members of the *Desmochitina* genus, whose first arrival in the palynological record coincides with the upper middle Arenig (Paris *et al.* 1999) or the datum of the third stage of the Ordovician global

chronostratigraphy, at *c*. 472 Ma (Cooper & Sadler 2004). Molyneux (1998) reviewed the work of Downie *et al.* (1971), concluding that the condition of microfossils identified as chitinozoans in the early work would not allow unequivocal assignation of a species or genus and thus that palynological evidence presented by Downie *et al.* (1971) for Arenig-age deposition of the Macduff Slates was not robust. Molneux (1998) however, did identify an archritarch described by Downie *et al.* (1971) as *Veryhachium lairdii*, whose first appearance in the palynological record occurs in the Tremadoc, at *c*. 483 (Servais *et al.* 2007) but whose presence continues well into the Arenig (S. G. Molyneux pers. comm.).

The controversial oldest deposition age of *c*. 472 Ma (Cooper & Sadler 2004) promoted by Downie *et al.* (1971) has often been dismissed on the grounds that it does not fit with active mountain building at that time. Sutton & Watson (1955) considered the sedimentary sequence preserved between Boyne Bay and Macduff to record an evolution in the environment of sedimentation, the decreasing calcareous and increasing coarse clastic sediment component indicating the emergence of a landmass. They stated that 'at the time of deposition of the upper Dalradian, the Caledonian movements had already begun' and that the material that constitutes the upper Dalradian sediments 'might have been derived from newly uplifted ridges' (Sutton & Watson 1955, p. 131). They matched the sediment sequence and sedimentary structures of the upper Dalradian with Oligocene and younger sediments of the Northern Apennines, a region that, from Miocene times, has seen extension and collapse of an orogenic edifice (cf. Carmignani *et al.* 1994; Barchi *et al.* 1998).

The model we have proposed for Grampian orogenesis certainly endorses Grampian-age deposition of the uppermost Dalradian (Whitehills and Boyndie Bay Groups and Macduff Slates) in a synorogenic (extensional) setting. The robust oldest deposition age of *c*. 483 Ma for the microfossil-bearing Macduff Slates does not discount deposition of the Macduff Slates during SZ_{topE} and $M_{Grampian}$, as required by our model. Evidence for or against a post-472 Ma Arenig age for the Macduff Slates will bear heavily on the validity of the model here presented.

Age of the Boyndie Syncline. A major requirement of the model presented here is that the Boyndie Syncline and related folds formed during the regional Buchan-type metamorphism. The results of our work are consistent with the structural age given to the Boyndie Syncline by Johnson & Stewart (1960), Johnson (1962) and Fettes (1970) and its development during the latest stages of the regional

metamorphism. Treagus & Roberts (1981), following Sutton & Watson (1956), assigned the Boyndie Syncline and related folds an early structural timing that pre-dated regional metamorphism. Treagus & Roberts (1981), as we have, observed a simpler structural history on the gently-dipping eastern limb of the Boyndie Syncline than that recorded in the steeper-dipping western limb. They argued that an absence of 'D_2' deformation (our SZ_{topE}) was related to differing strain response offered by the separate limbs of a pre-existing fold structure (the Boyndie Syncline). Late folding imparted on a sequence deposited during the SZ_{topE} episode would take the appearance of an early fold generation and can explain the absence of pre-SZ_{topE} structures east of Whitehills. The metamorphic (Fig. 2a), shear zone and magmatic patterns (Fig. 3) of the eastern part of the Grampian Terrane define the axial trace of the Boyndie Syncline. A SZ_{topE} age for emplacement of Grampian gabbros into the flat-lying (Fettes 1970; Droop & Charnley 1985) regional shear network and for development of much of the regional metamorphic pattern calls into question claims for pre-SZ_{topE} formation of the Boyndie Syncline.

Conclusion

A new tectonic model for development of the Buchan Block and the adjoining Barrovian-type units of the Grampian Terrane, Scotland, has been proposed on the basis of field mapping, microstructural analysis, metamorphic petrology and mafic magma geochemistry. The model proposes that metamorphic heating to produce the Buchan-type units and neighbouring Barrovian-type assemblages was associated with lithospheric-scale extension and the emplacement of mafic magmas sourced from decompression melting of the asthenosphere beneath lithosphere less than 70 km thick. Lithospheric-scale extension followed initiation of Grampian orogenesis by lithospheric-scale thickening and was itself followed by renewed thickening of the lithosphere, imposed on a crustal section still hot from extension-related heating. A large proportion of the strain associated with the lithospheric-scale shortening and extension episodes was accommodated by movement across a gently-dipping, mid-crustal detachment, manifest as the gabbro-bearing shear zones of the Buchan Block described by Ashcroft *et al.* (1984). The Buchan Block comprised the hanging wall to this detachment, whereas Barrovian-type units were produced in the footwall. In the model, translation of the Buchan hanging wall relative to metamorphic heat sources (magmas) in the footwall can account for differences observed in the metamorphic

pressure-temperature history of the Buchan Block relative to the neighbouring Barrovian-type units. Repeated movements of opposing polarity across the mid-crustal detachment resulted in abandonment of high-grade lenses of Grenvillean basement within the Dalradian sequence.

According to the new model, the regional metamorphic pattern (Barrovian- and Buchan-type metamorphism) was first established during top-to-the-east shear across the Portsoy-Duchray Hill Lineament and emplacement of the Grampian gabbros into the shear zones. The uppermost regions of the Dalradian (the Whitehills and Boyndie Bay Groups and the Macduff Slates) were deposited during the syn-orogenic extension that saw Grampian bimodal magmatism and regional metamorphic heating. The Boyndie Syncline represents a late structure (cf. Johnson 1960; Johnson & Stewart 1962), developed during the second Grampian-age thickening episode to affect the Grampian Terrane, and post-dates Grampian bimodal magmatism and regional metamorphic heating.

References

AGOSTINI, S., DOGLIONI, C., INNOCENTI, F., MANETTI, P., TONARINI, S. & SAVAŞÇIN, M. Y. 2007. The transition from subduction-related to intraplate Neogene magmatism in the Western Anatolia and Aegean area. *In*: BECCALUVA, L., BIANCHINI, G. & WILSON, M. (eds) *Cenozoic Magmatism in the Mediterranean Area*. Geological Society of America, Colorado, Special Paper, **418**, 1–16.

AHMED-SAID, Y. & TANNER, P. W. G. 2000. *P–T* conditions during emplacement, and D2 regional metamorphism, of the Ben Vuirich Granite, Perthshire, Scotland. *Mineralogical Magazine*, **64**, 737–753.

ASHCROFT, W. A., KNELLER, B. C., LESLIE, A. G. & MUNRO, M. 1984. Major shear zones and autochthonous Dalradian in the north–east Scottish Caledonides. *Nature*, **310**, 760–762.

ASHWORTH, J. R. 1975. The sillimanite zones of the Huntly-Portsoy area in the north–east Dalradian, Scotland. *Geological Magazine*, **112**, 113–224.

BAKER, A. J. 1985. Pressures and temperatures of metamorphism in the Eastern Dalradian of Scotland. *Journal of the Geological Society, London*, **142**, 137–148.

BAKER, A. J. 1987. Models for the tectonothermal evolution of the eastern Dalradian. *Journal of Metamorphic Geology*, **5**, 101–118.

BARCHI, M. R., DE FEYTER, A. J., MAGNANI, M. B., MINELLI, G., PIALLI, G. & SOTERA, B. M. 1998. Extensional tectonics in the Northern Apennines (Italy): evidence from the Crop03 deep seismic reflection line. *Memorie della Societá Geologica Italiana*, **52**, 527–538.

BARROW, G. 1893. On an intrusion of muscovite-biotite gneiss in the southeastern Highlands of Scotland and its accompanying metamorphism. *Quarterly Journal of the Geological Society, London*, **49**, 330–358.

BARROW, G. 1912. On the geology of Lower Dee-side and the southern Highland Border. *Geological Association of London Proceedings*, **23**, 274–290.

BEDDOE-STEPHENS, B. 1990. Pressures and temperatures of Dalradian metamorphism and the andalusite-kyanite transformation in the Northeast Grampians. *Scottish Journal of Geology*, **26**, 3–14.

BELTRANDO, M., HERMANN, J., LISTER, G. S. & CAMPAGNONI, R. 2007. On the evolution of orogens: pressure cycles and deformation mode switches. *Earth and Planetary Science Letters*, **256**, 372–388.

BELTRANDO, M., LISTER, G. S., HERMANN, J., FORSTER, M. A. & CAMPAGNONI, R. 2008. Deformation mode switches in the Penninic units of the Urtier Valley (Western Alps): evidence for a dynamic orogen. *Journal of Structural Geology*, **30**, 194–219.

BOGER, S. D. & HANSEN, D. 2004. Metamorphic evolution of the Georgetown Inlier, northeast Queensland, Australia; evidence for an accreted Paleoproterozoic terrane? *Journal of Metamorphic Geology*, **22**, 511–527.

CARMIGNANI, L., DECANDIA, F. A., DISPERATI, L., FANTOZZI, P. L., LAZZAROTTO, A., LIOTTA, D. & MECCHERI, M. 1994. Tertiary extensional tectonics in Tuscany (Northern Apennines, Italy). *Tectonophysics*, **238**, 295–315.

CARTY, J. P. 2001. *Deformation, magmatism and metamorphism in the Portsoy shear zone, North–East Scotland*. PhD thesis, University of Derby.

CARTY, J. P., CONNELLY, J. N., GALE, J. & HUDSON, N. F. C. 2002. Kinematics and timing of deformation in the Portsoy shear zone. *In*: *Tectonic Studies Group Annual Meeting Abstracts*. University of Leicester, Leicester, 54.

CHINNER, G. A. 1966. The distribution of pressure and temperature during Dalradian metamorphism. *Quarterly Journal of the Geological Society, London*, **122**, 159–181.

CHINNER, G. A. 1980. Kyanite isograds of Grampian metamorphism. *Journal of the Geological Society, London*, **137**, 35–39.

CHINNER, G. A. & HESELTINE, F. J. 1979. The Grampide andalusite/kyanite isograd. *Scottish Journal of Geology*, **15**, 117–127.

CONDIE, K. C. 1993. Chemical composition and evolution of the upper continental crust: contrasting results from surface samples and shales. *Chemical Geology*, **104**, 1–37.

COOPER, R. A. & SADLER, P. M. 2004. The Ordovician period. *In*: GRADSTEIN, F. M., OGG, J. G. & SMITH, A. G. (eds) *A Geological Time Scale 2004*. Cambridge University Press, Cambridge, 165–187.

COX, K. G., BELL, J. D. & PANKHURST, R. J. 1979. *The Interpretation of Igneous Rocks*. Allen & Unwin, London.

DEMPSTER, T. J., HUDSON, N. F. C. & ROGERS, G. 1995. Metamorphism and cooling of the NE Dalradian. *Journal of the Geological Society, London*, **152**, 383–390.

DEMPSTER, T. J., ROGERS, G. *ET AL.* 2002. Timing of deposition, orogenesis and glaciation within the Dalradian rocks of Scotland: constraints from U–Pb ages. *Journal of the Geological Society, London*, **159**, 83–94.

DOWNIE, C., LISTER, T. R., HARRIS, A. L. & FETTES, D. J. 1971. *A Palynological Investigation of the Dalradian Rocks of Scotland*. Institute of Geological Sciences Report, HMSO, London, **71/9**.

DRAUT, A. E. & CLIFT, P. D. 2001. Geochemical evolution of arc magmatism during arc-continent collision, South Mayo, Ireland. *Geology*, **29**, 543–546.

DROOP, G. T. R. & CHARNLEY, N. R. 1985. Comparative geobarometry of pelitic hornfelses associated with the Newer Gabbros: a preliminary study. *Journal of the Geological Society, London*, **142**, 53–62.

ELLES, G. L. 1931. Notes on the Portsoy coastal district. *Geological Magazine*, **68**, 24–34.

ELLES, G. L. & TILLEY, C. E. 1930. Metamorphism in relation to structure in the Scottish Highlands. *Transactions of the Royal Society of Edinburgh*, **56**, 621–646.

FETTES, D. J. 1970. The structural and metamorphic state of the Dalradian rocks and their bearing on the age of emplacement of the basic sheet. *Scottish Journal of Geology*, **6**, 108–118.

FETTES, D. J. & MUNRO, M. 1989. Age of the Blackwater mafic and ultramafic intrusion, Banffshire. *Scottish Journal of Geology*, **25**, 105–111.

FETTES, D. J., GRAHAM, C. M., HARTE, B. & PLANT, J. A. 1986. Lineaments and basement domains: an alternative view of Dalradian evolution. *Journal of the Geological Society, London*, **143**, 453–464.

FETTES, D. J., LESLIE, A. G., STEPHENSON, D. & KIMBELL, S. F. 1991. Disruption of Dalradian stratigraphy along the Portsoy Lineament from new geological and magnetic surveys. *Scottish Journal of Geology*, **27**, 57–73.

FORSTER, M. A. & LISTER, G. S. 2008. Tectonic sequence diagrams and the structural evolution of schists and gneisses in multiply deformed terranes. *Journal of the Geological Society, London*, **165**, 923–939.

FORSTER, M. A. & LISTER, G. S. 2009. Core complex related extension of the Aegean lithosphere initiated at the Eocene-Oligocene transition. *Journal of Geophysical Research: Solid Earth*, **114**, B02401.

FRIEDRICH, A. M., BOWRING, S. A., MARTIN, M. W. & HODGES, K. V. 1999. Short-lived continental magmatic arc at Connemara, western Irish Caledonides: implications for the age of the Grampian Orogeny. *Geology*, **27**, 27–30.

GOODMAN, S. 1994. The Portsoy-Duchray Hill Lineament: a review of the evidence. *Geological Magazine*, **131**, 407–415.

GOODMAN, S. & WINCHESTER, J. A. 1993. Geochemical variations within metavolcanic rocks of the Dalradian Farragorn Beds and adjacent formations. *Scottish Journal of Geology*, **29**, 131–141.

GRAHAM, C. M. 1976. Petrochemistry and tectonic significance of Dalradian metabasaltic rocks of the SW Scottish Highlands. *Journal of the Geological Society, London*, **132**, 61–84.

HALLIDAY, A. N., GRAHAM, C. M., AFTALION, M. & DYMOKE, P. 1989. The depositional age of the Dalradian Supergroup: U–Pb and Sm–Nd isotopic studies of the Tayvallich Volcanics, Scotland. *Journal of the Geological Society, London*, **146**, 3–6.

HARMON, R. S. 1983. Oxygen and Strontium isotope evidence regarding the role of continental crust in the origin and evolution of the British Caledonian granites. *In*: ATHERTON, M. P. & GRIBBLE, C. D. (eds) *Migmatites, Melting and Metamorphism*. Shiva, Nantwich, 62–79.

HARTE, B. & HUDSON, N. F. C. 1979. Pelite facies series and the temperatures and pressures of Dalradian metamorphism in E Scotland. *In*: HARRIS, A. L., HOLLAND, C. H. & LEAKE, B. E. (eds) *The Caledonides of the British Isles – Reviewed*. Geological Society, London, Special Publications, **8**, 323–337.

HUDSON, N. F. C. 1980. Regional metamorphism of some Dalradian pelites in the Buchan area, NE Scotland. *Contributions to Mineralogy and Petrology*, **73**, 39–51.

HUDSON, N. F. C. 1985. Conditions of Dalradian metamorphism in the Buchan area, NE Scotland. *Journal of the Geological Society, London*, **142**, 63–76.

JACQUES, J. M. & REAVY, R. J. 1984. Caledonian plutonism and major lineaments in the SW Scottish Highlands. *Journal of the Geological Society, London*, **151**, 955–969.

JOHNSON, M. R. W. 1962. Relations of movement and metamorphism in the Dalradians of Banffshire. *Transactions of the Edinburgh Geological Society*, **19**, 29–64.

JOHNSON, M. R. W. & STEWART, F. H. 1960. On Dalradian structures in north–east Scotland. *Transactions of the Edinburgh Geological Society*, **18**, 94–103.

JOHNSON, T. E., HUDSON, N. F. C. & DROOP, G. T. R. 2003. Evidence for a genetic granite-migmatite link in the Dalradian of NE Scotland. *Journal of the Geological Society, London*, **160**, 447–457.

KAY, R. W. & GAST, P. W. 1973. The rare earth content and origin of alkali-rich basalts. *Journal of Geology*, **81**, 653–682.

KELEMEN, P. B., JOHNSON, K. T., KINZLER, R. J. & IRVING, A. J. 1990. High-field-strength element depletions in arc basalts due to mantle-magma interaction. *Nature*, **345**, 521–524.

KLEMME, S. & O'NEILL, H. ST. C. 2000. The near-solidus transition from garnet lherzolite to spinel lherzolite. *Contributions to Mineralogy and Petrology*, **138**, 237–248.

KNELLER, B. C. & AFTALION, M. 1987. The isotopic and structural age of the Aberdeen Granite. *Journal of the Geological Society, London*, **144**, 717–721.

KNELLER, B. C. & LESLIE, A. G. 1984. Amphibolite facies metamorphism in shear zones in the Buchan area of NE Scotland. *Journal of Metamorphic Geology*, **2**, 83–94.

KRETZ, R. 1983. Symbols for rock-forming minerals. *American Mineralogist*, **68**, 277–279.

LAMBERT, R. S. J. & MCKERROW, W. S. 1976. The Grampian Orogeny. *Scottish Journal of Geology*, **12**, 271–292.

LANDENBERGER, B. & COLLINS, W. J. 1976. Derivation of A-type granites from a dehydrated charnockitic lower crust: evidence from the Chaelundi Complex, Eastern Australia. *Journal of Petrology*, **37**, 145–170.

LESLIE, A. G. 1984. Field relations in the north-eastern part of the Insch mafic igneous mass, Aberdeenshire. *Scottish Journal of Geology*, **20**, 215–235.

MCDONALD, R., FETTES, D. J., STEPHENSON, D. & GRAHAM, C. M. 2005. Basic and ultrabasic volcanic rocks from the Argyll Group (Dalradian) of NE Scotland. *Scottish Journal of Geology*, **41**, 159–174.

MCDONOUGH, W. F. & SUN, S.-S. 1995. The composition of the Earth. *Chemical Geology*, **120**, 223–253.

MACGREGOR, S. M. & ROBERTS, J. L. 1963. Dalradian pillow lavas, Ardwell Bridge, Banffshire. *Geological Magazine*, **100**, 17–23.

MANTLE, G. W. & COLLINS, W. J. 2008. Quantifying crustal thickness variations in evolving orogens: correlation between arc basalt composition and Moho depth. *Geology*, **36**, 87–90.

MIDDLEMOST, E. A. K. 1975. The basalt clan. *Earth Science Reviews*, **11**, 337–364.

MIYASHIRO, A. 1978. Nature of alkalic volcanic rock series. *Contributions to Mineralogy and Petrology*, **66**, 91–104.

MOLYNEUX, S. G. 1998. An upper Dalradian microfossil reassessed. *Journal of the Geological Society, London*, **155**, 741–743.

MUNRO, M. & GALLAGHER, J. W. 1984. Disruption of the 'Younger Basic' masses in the Huntly-Portsoy area, Grampian region. *Scottish Journal of Geology*, **20**, 361–382.

OLIVER, G. J. H. 2001. Reconstruction of the Grampian episode in Scotland: its place in the Caledonian Orogeny. *Tectonophysics*, **332**, 23–49.

OLIVER, G. J. H., CHEN, F., BUCHWALDT, R. & HEGNER, E. 2000. Fast tectonometamorphism and exhumation in the type area of the Barrovian and Buchan zones. *Geology*, **28**, 459–462.

OLIVER, G. J. H., MARTIN, M. W. & BANKS, G. 2002. Origin of the tectonised 470 Ma 'Older Basic' Complex, NE Scotland. *In*: *Tectonic Studies Group Annual Meeting Abstracts*. University of Leicester, Leicester, 55.

O'NEILL, H. ST. C. 1981. The transition between spinel lherzolite and garnet lherzolite, and its use as a geobarometer. *Contributions to Mineralogy and Petrology*, **77**, 195–184.

PANKHURST, R. J. 1970. The geochronology of the basic igneous complexes. *Scottish Journal of Geology*, **6**, 83–107.

PARIS, F., GRAHN, Y., NESTOR, V. & LAKOVA, I. 1999. A revised chitonozoan classification. *Journal of Paleontology*, **73**, 549–570.

PEARCE, J. 1983. Role of the subcontinental lithosphere in magma genesis at active continental margins. *In*: HAWKESWORTH, C. J. & NORRY, M. J. (eds) *Continental Basalts and Mantle Xenoliths*. Shiva, Nantwich, 230–249.

PIDGEON, R. T. & AFTALION, M. 1978. Cogenetic and inherited zircon U–Pb systems in granites: Palaeozoic granites of Scotland and England. *In*: BOWES, D. R. & LEAKE, B. E. (eds) *Crustal Evolution in Northwestern Britain and Adjacent Regions*. Seel House Press, Liverpool, 183–220.

PIDGEON, R. T. & COMPSTON, W. 1992. A SHRIMP ion microprobe study of inherited and magmatic zircons from four Scottish Caledonian granites. *Transactions of the Royal Society of Edinburgh: Earth Sciences*, **83**, 473–483.

PIERCEY, S. J., MORTENSEN, J. K., MURPHY, D. C., PARADIS, S. & CREASER, R. A. 2002. Geochemistry and tectonic significance of alkalic mafic magmatism in the Yukon-Tanana terrane, Finlayson Lake region, Yukon. *Canadian Journal of Earth Sciences*, **39**, 1729–1744.

RAMSAY, D. M. & STURT, B. A. 1979. The status of the Banff nappe. *In*: HARRIS, A. L., HOLLAND, C. H. & LEAKE, B. E. (eds) *The Caledonides of the British Isles – Reviewed*. Geological Society, London, Special Publications, **8**, 145–151.

READ, H. H. 1919. The two magmas of Strathbogie and lower Banffshire. *Geological Magazine*, **56**, 364–371.

READ, H. H. 1923. *Geology of the Country Round Banff, Huntly and Turriff*. Memoir of the Geological Survey, Scotland. HMSO, Edinburgh, **Sheets 86 & 96**.

READ, H. H. 1952. Metamorphism and migmatisation in the Ythan Valley, Aberdeenshire. *Transactions of the Edinburgh Geological Society*, **15**, 265–279.

READ, H. H. 1955. The Banff Nappe: an interpretation of the structure of the Dalradian rocks of north–east Scotland. *Proceedings of the Geologists' Association*, **66**, 1–29.

READ, H. H. & FARQUHAR, O. C. 1956. The Buchan Anticline of the Banff Nappe of Dalradian Rocks in north–east Scotland. *Quarterly Journal of the Geological Society, London*, **112**, 131–156.

RICHARDS, S. W. & COLLINS, W. J. 2004. Growth of wedge-shaped plutons at the base of active half-grabens. *Transactions of the Royal Society of Edinburgh: Earth Sciences*, **95**, 309–317.

ROGERS, G., DEMPSTER, T. J., BLUCK, B. J. & TANNER, P. W. G. 1989. A high-precision U–Pb age for the Ben Vuirich granite: implications for the evolution of the Scottish Dalradian Supergroup. *Journal of the Geological Society, London*, **146**, 789–798.

RUDNICK, R. L. & FOUNTAIN, D. M. 1995. Nature and composition of the continental crust: a lower crustal perspective. *Reviews of Geophysics*, **33**, 267–309.

SAUNDERS, A. D., NORRY, M. J. & TARNEY, J. 1991. Fluid influence on the trace element compositions of subduction zone magmas. *Royal Society of London Philosophical Transactions: Physical Sciences and Engineering*, **335**, 377–392.

SEGHEDI, I., DOWNES, H. *ET AL.* 2004. Neogene-Quaternary magmatism and geodynamics in the Carpathian-Pannonian region: a synthesis. *Lithos*, **72**, 117–146.

SERVAIS, T., VECOLI, M., LI, J., MOLYNEUX, S. G., RAEVSKAYA, E. G. & RUBINSTEIN, C. V. 2007. The acritarch genus *Veryhachium* Deunff 1954: taxonomic evaluation and first appearance. *Palynology*, **31**, 191–203.

SINGER, B. S. & MYERS, J. D. 1990. Intra-arc extension and magmatic evolution in the central Aleutian arc, Alaska. *Geology*, **18**, 1050–1053.

STEPHENSON, D. & GOULD, D. 1995. *British Regional Geology: The Grampian Highlands*. HMSO, London.

STURT, B. A., RAMSAY, D. M., PRINGLE, I. R. & TEGGIN, D. E. 1977. Precambrian gneisses in the Dalradian sequence of northeast Scotland. *Journal of the Geological Society, London*, **134**, 41–44.

SUN, S.-S. & MCDONOUGH, W. F. 1989. Chemical and isotopic systematics of oceanic basalts: implications for mantle composition and processes. *In*: SAUNDERS, A. D. & NORRY, M. J. (eds) *Magmatism in the Ocean Basins*. Geological Society, London, Special Publications, **42**, 313–345.

SUTTON, J. & WATSON, J. 1955. The deposition of the Upper Dalradian rocks of the Banffshire coast. *Proceedings of the Geologists' Association*, **66**, 101–133.

SUTTON, J. & WATSON, J. 1956. The Boyndie Syncline of the Dalradian of the Banffshire coast. *Quarterly Journal of the Geological Society, London*, **112**, 103–130.

TANNER, P. W. G. 1996. Significance of the early fabric in the contact metamorphic aureole of the 590 Ma Ben Vuirich Granite, Perthshire, Scotland. *Geological Magazine*, **133**, 683–695.

TANNER, P. W. G., LESLIE, A. G. & GILLESPIE, M. R. 2006. Structural setting and petrogenesis of the Ben Vuirich Granite Pluton of the Grampian Highlands: a pre-orogenic, rift-related intrusion. *Scottish Journal of Geology*, **42**, 113–136.

THOMPSON, R. N., DEWEY, J. F. & MUNRO, M. 1985. Model for Grampian tract evolution: discussion and reply. *Nature*, **314**, 562.

TREAGUS, J. E. & ROBERTS, J. L. 1981. The Boyndie Syncline, a D_1 structure in the Dalradian of Scotland. *Geological Journal*, **16**, 125–135.

TREWIN, N. H. & ROLLIN, K. E. 2002. Geological history and structure of Scotland. *In*: TREWIN, N. H. (ed.) *The Geology of Scotland*. Geological Society, London, 1–26.

UTO, K., HOANG, N. & MATSUI, K. 2004. Cenozoic lithospheric extension induced magmatism in Southwest Japan. *Tectonophysics*, **393**, 281–299.

VAN DE KAMP, C. 1970. The green beds of the Scottish Dalradian series: geochemistry, origin and metamorphism of mafic sediments. *Journal of Geology*, **78**, 281–303.

WANG, K.-L., CHUNG, S.-L., CHEN, C.-H, SHINJO, R., YANG, T. F. & CHEN, C.-H. 1999. Post-collisional magmatism around northern Taiwan and its relation with opening of the Okinawa Trough. *Tectonophysics*, **308**, 363–376.

WELLINGS, S. A. 1998. Timing of deformation associated with the syn-tectonic Dawros-Currywongaun-Doughruagh Complex, NW Connemara, western Ireland. *Journal of the Geological Society, London*, **155**, 25–37.

WILSON, J. R. & LEAKE, B. E. 1972. The petrochemistry of the epidiorites of the Tayvallich Peninsula, North Knapdale, Argyllshire. *Scottish Journal of Geology*, **8**, 215–252.

ZENK, M. & SCHULZ, B. 2004. Zoned Ca-amphiboles and related *P*–*T* evolution in metabasites from the classical Barrovian metamorphic zones in Scotland. *Mineralogical Magazine*, **68**, 769–786.

ZHOU, X. M. & LI, W. X. 2000. Origin of Mesozoic igneous rock in Southeastern China: implications for lithosphere subduction and underplating of mafic magmas. *Tectonophysics*, **326**, 269–287.